Freshwater and Heat Changes in the North and South Pacific Oceans between the 1960s and 1985–94

ANNIE P. S. WONG

Institute of Antarctic and Southern Ocean Studies, University of Tasmania, Hobart, Australia

NATHANIEL L. BINDOFF

Antarctic Cooperative Research Centre, Hobart, Australia

JOHN A. CHURCH

Antarctic Cooperative Research Centre and CSIRO Division of Marine Research, Hobart, Australia

(Manuscript received 28 February 2000, in final form 25 July 2000)

ABSTRACT

Comparisons of hydrographic conditions in the North and South Pacific Oceans in the 1960s and 1985–94 have been made along five World Ocean Circulation Experiment sections. Below the seasonal mixed layer, statistically significant temporal differences in salinity and temperature have been detected in the water masses that occur in the upper 2000 dbar of the water column. These water mass property differences have been used to estimate the freshwater and heat storage trends in the Pacific over the study period. Along 24°N, 10°N, and 17°S, where either North Pacific Intermediate Water or Antarctic Intermediate Water is present, the upper waters have increased in salinity, while the intermediate and deep waters have decreased in salinity. Although the depth-integrated salinity changes observed along these sections are small, the regional redistribution of freshwater associated with the water mass changes is significant and implies significant redistribution of surface freshwater fluxes over the Pacific. Heat loss has occurred along 47°N and 17°S, but significant warming has occurred along 24° and 10°N, giving the Pacific a net heat gain of 1.79×10^8 J m^{-2}. The resulting steric sea level change for the area in the Pacific between 60°N and 31.5°S over the roughly 20-yr study period is estimated to be a rise of 0.85 mm yr^{-1}, consistent with those in existing literature, but larger than that estimated from numerical models reported in the Intergovernmental Panel on Climate Change Second Assessment Report.

1. Introduction

The world's oceans exhibit variability on various timescales. Below the surface mixed layer, decadal changes in ocean properties are more prominent, and can reveal significant trends in the climate system. For example, by reviewing the recent changes in the North Atlantic Ocean, Dickson et al. (1996) proposed that winter convection at the three convective renewal sites of the North Atlantic: the Greenland–Iceland Sea, the Labrador Sea, the Sargasso Sea, evolved in phase but at different signs during this century, and that this decadal evolution was driven by the North Atlantic oscillation (NAO) of the atmosphere. Variability of Labrador Sea Water (LSW) was shown to depend on the NAO. Koltermann et al. (1999) used a set of repeated oceanwide hydrographic sections (including those from Roemmich and Wunsch 1984; Read and Gould 1992; Parrilla et al. 1994) to study natural interdecadal variability of the intermediate layers of the North Atlantic, and related LSW variability to the varying intensity of the meridional overturning circulation of the North Atlantic Ocean.

In the Pacific, the few repeat hydrographic transects to date that can be used to study large-scale oceanic changes are mostly restricted to the western ocean basins. In the North Pacific, the Japanese Meteorological Agency has been surveying the 137°E meridian since 1967, and the dataset has been used by many authors to study interannual variability of various water masses, such as North Pacific Subtropical Mode Water (STMW) and North Pacific Intermediate Water (NPIW; e.g., Suga et al. 1989; Qiu and Joyce 1992; Suga and Hanawa 1995; Shuto 1996). In the South Pacific, the western portions of the 1967 SCORPIO lines along 28° and 43°S were repeated in 1989/90, and revealed warming of waters in the main thermocline and in the intermediate

Corresponding author address: Dr. Annie P. Wong, NOAA/PMEL/OCRD, 7600 Sand Point Way, Bldg. 3, Seattle, WA 98115-6349.
E-mail: awong@pmel.noaa.gov

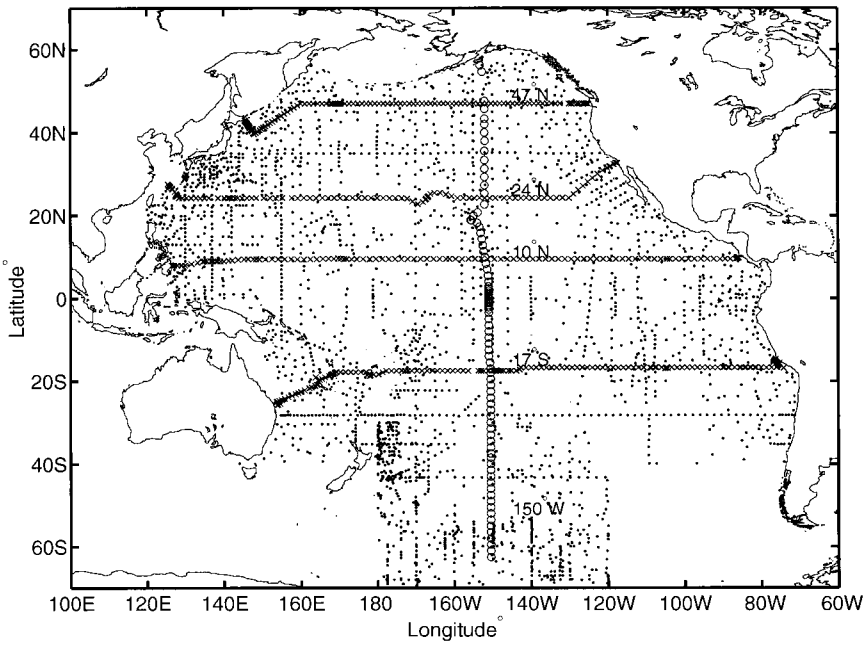

FIG. 1. The cruise tracks of the five WOCE sections: P1 at 47°N, P3 at 24°N, P4 at 10°N, P21 at 17°S, and P16 at 150°W, and the locations of the historical hydrographic casts that have been used in this study.

levels, in the Tasman Sea between Australia and New Zealand (Bindoff and Church 1992). Johnson et al. (1994) studied three hydrographic sections across the Samoa Passage, spanning 25 yr, and detected decadal-scale variability in modified North Atlantic Deep Water. More observed changes in Subantarctic Mode Water (SAMW) and Antarctic Intermediate Water (AAIW) in the southwest Pacific along 170°W and 35°S have been presented by Johnson and Orsi (1997).

The North and South Pacific Oceans combined contain almost half of the world ocean volume. Yet relative to the North Atlantic, few studies have been done on basin-scale changes in the ocean interior. Wong et al. (1999) reported large-scale freshening of intermediate waters in the Pacific and Indian Oceans, based on hydrographic observations along four zonal Pacific sections from the World Ocean Circulation Experiment (WOCE), and results from Bindoff and Church (1992) and Bindoff and McDougall (2000). In this paper, we expand on the Pacific observations of Wong et al. (1999), and examine the large-scale decadal changes in the North and South Pacific Oceans between the two decades, the 1960s and 1985–94. We then use the differences in salinity and temperature to estimate the changes in freshwater and heat contents in the Pacific Ocean.

2. Data and method

Five WOCE sections that are located in regions with dense historical hydrographic data have been selected for this comparative study. These five WOCE sections were sampled in the decade 1985–94. Four out of the five sections are zonal transects and form the basis of our freshwater and heat estimations. The four zonal WOCE sections are P1 at 47°N (1985), P3 at 24°N (1985), P4 at 10°N (1989), and P21 at 17°S (1994). One meridional section that runs along the nominal longitude of 150°W, WOCE P16 (1991–92), has been used to provide supplementary observation on the intermediate layers of the Pacific Ocean. All five sections are now publicly available from the WOCE World Hydrographic Program Office (online at http://whpo.ucsd.edu).

The CTD data (in situ temperature IPTS-68, and salinity PSS-78) from the five WOCE sections were compared with historical hydrographic casts from two world datasets. Between 60°N and 40°S, 1914 full-depth casts (mainly Nansen casts) from the Reid and Mantyla Pacific database have been selected. South of 40°S, historical data from the Hydrographic Atlas of the Southern Ocean (Olbers et al. 1992) have been used, as the Olbers atlas contains the same Southern Ocean data points as the Reid and Mantyla database and more. All selected historical casts have been screened for outliers, which have subsequently been removed. Figure 1 shows the locations of the five WOCE sections and the historical casts used in this study.

These historical data span the years 1928–89, with the majority from the late 1960s (Fig. 2). The mean year of sampling of the historical casts is 1968, with a standard deviation of 7.5 yr. Hence the differences between

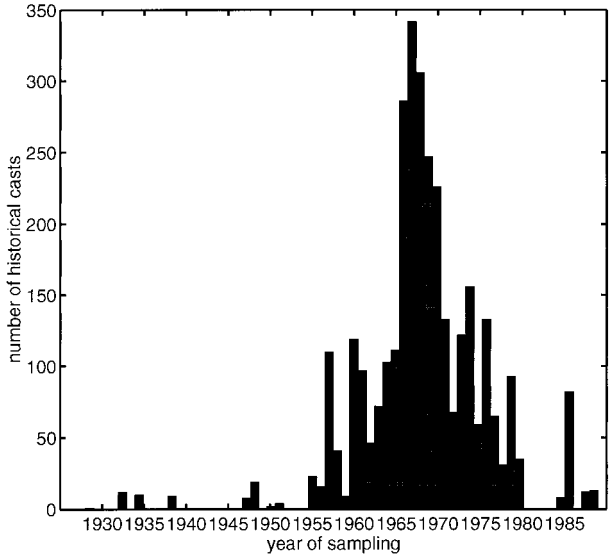

FIG. 2. The year distribution of the historical hydrographic casts that have been used in this study.

the historical data and the WOCE data can be treated as roughly 20 ± 7 yr differences.

For the historical casts that have been used for comparison along 47° and 24°N, the most frequent months of sampling coincide with the WOCE sampling seasons (August for 47°N, and May for 24°N). Hence the likelihood of seasonal aliasing in the observed temporal changes along 47° and 24°N is minimal. On the other hand, the sampling seasons of the historical casts that have been used for comparison along 10°N and 17°S are relatively more uniformly distributed throughout the year. Hence there is the possibility of seasonal aliasing in the comparisons (biased toward February–May for 10°N, and toward April–June for 17°S), especially for 10°N, where the strong seasonal cycle causes isopycnal displacements. However, the effects of seasonal variations in water mass properties are confined to the shallow mixed layers and are weak in the main thermocline. The meridional section P16 along 150°W was sampled over two years, and spanned the months between March and October. Seasonal bias is present but is different for the various subsections.

To compare the historical hydrographic data and the CTD data from the five WOCE sections, interpolations have been done so that the data points occupy common coordinates, vertically and laterally. Vertically, most historical measurements were taken from Nansen bottles at discrete depths. On the other hand, the modern WOCE data were obtained by continuous electronic conductive, temperature, depth (CTD) profilers. Hence the first interpolation step was to vertically subsample all WOCE CTD data at standard depths to imitate the vertical spacings between bottle samples. The historical data have also been interpolated to the standard depths. All data were subsequently labeled with neutral densities. Then temperature, salinity, and pressure on standard neutral surfaces were obtained by quadratic interpolation that retained the curvature of the vertical profiles (Jackett and McDougall 1997).

The historical data were then objectively mapped to the WOCE coordinates. The objective estimate Ψ_{grid} of a property field at the desired grid is given by $\Psi_{\text{grid}} = \overline{\Psi} + w(\Psi - \overline{\Psi})$, where Ψ denotes the group of historical data used in the estimate, and $\overline{\Psi}$ denotes the underlying mean field of the data. The coefficient $w = C_{dg}\, C_{dd}^{-1}$ is the data–grid covariance normalized by the data–data covariance. The covariance function is assumed to be Gaussian.

The coefficient matrix takes into account the signal variance and the noise variance of the property field Ψ. The signal variance $\text{var}(s_\Psi)$ is estimated by

$$\text{var}(s_\Psi) = \frac{1}{n}\sum_{i=1}^{n}(\Psi_i - \overline{\Psi})^2,$$

where n is the number of historical data points on the neutral surface. The noise variance $\text{var}(\eta_\Psi)$, also known as the a priori noise, is estimated by

$$\text{var}(\eta_\Psi) = \frac{1}{2n}\sum_{i=1}^{n}(\Psi_i - \Psi_j)^2,$$

where Ψ_i and Ψ_j are pairs of closest historical data points on the neutral surface.

A two-step mapping technique has been employed: the first step uses a set of long length scales to map the historical data; the second step uses a set of short length scales to map the residuals from the first step. The long scales are typically around 20° longitude and 15° latitude, and the short scales are typically around 7° longitude and 5° latitude. The final estimated fields at the WOCE coordinates are the sums of the long scale estimates and the short scale estimates.

Objective mapping has been done on neutral surfaces to preserve oceanic properties (Lozier et al. 1994). However, some objective estimates in the top 200 dbar give unrealistic variations in density. In addition, inversions in the top 200 dbar are common. This is because the historical data have been collected over many seasons and many years, so the noise levels associated with the property fields are large in the top 200 dbar that contains the seasonal mixed layer. Also, in the deep ocean below about 4000 dbar, very few historical data exist. Hence the objective estimates below 4000 dbar are usually unrealistic as well. In this study, the parts of the water column where objective estimates are unrealistic and where pressure inversions occur, have been excluded from the discussion.

3. Temporal changes in salinity and temperature

Traditionally, comparisons of hydrographic data have been done on isobars. However, viewing temporal differences on isobars is inadequate for diagnosing the

cause of the change, because differences on isobars contain the effects of both true water mass property changes and isopycnal movements. On the other hand, salinity (S) and potential temperature (θ) differences observed on isopycnals can be due to lateral gyre wobble, or can be due to real water mass property changes as a result of altered sea surface conditions. In the case of a real θ–S property change, information provided by observations on isopycnals alone is inadequate for interpreting the cause of the change. The most thorough analysis of water mass changes therefore requires the complementary views from the two reference frames: on isobars and on isopycnals.

Salinity and temperature properties of water masses are initially set at the sea surface, and are then injected into the ocean interior by subduction. The properties of a water mass are then modified by mixing along its spreading path. However, in the ocean interior, the transfer of properties is dominated more by advection along isopycnals than by mixing processes. Therefore, as a first approximation, interior water mass differences are assumed to be caused by changes in sea surface conditions at the source regions.

In a study concerning the ocean's response to a warmed atmosphere, Church et al. (1991) pointed out the counterintuitive feature that, in a ''warming without salinity change'' scenario, the effect of warmed water subducted into a thermocline (where salinity decreases with increasing depth/density) would be to cause an observed cooling (and corresponding freshening) on isopycnals. Bindoff and McDougall (1994) expanded this concept and formalized three ''pure'' processes that could result in subsurface changes in S and θ. These three idealized subduction processes are termed ''pure warming (or cooling),'' ''pure freshening (or salination),'' and ''pure heaving.'' In *pure warming*/*cooling* and *pure freshening*/*salination*, changes in water mass property can lead to different changes on neutral surfaces, depending on the slope of the θ–S curve. In *pure heaving*, water mass property change is absent, and so differences observed on isobars are all due to vertical movements of isopycnals.

Temporal changes in salinity and temperature are here examined on isopycnal surfaces as well as isobaric surfaces. Neutral density (kg m^{-3}, hereafter denoted by γ^n, omitting the units) is used because the ambiguity of choosing reference pressures is eliminated. Here $S'|_n$ and $\theta'|_n$ denote temporal changes of salinity and temperature on neutral surfaces. The $S'|_z$ and $\theta'|_z$ denote temporal changes of salinity and temperature on isobars. The N' denotes temporal changes in depth of the neutral surfaces. Differences have been obtained by subtracting objectively mapped historical values from the WOCE values. Hence negative differences mean decreases over time. In the case of isopycnal depths, a negative difference means a deepening of isopycnals over time. The following sections give detailed descriptions of temporal changes along the four zonal sections, because they form the basis for calculating the freshwater and heat budgets. Results along the meridional WOCE P16 section at 150°W are discussed as supplement to the changes observed in the intermediate layers.

a. Spatial pattern of the temporal changes

1) DIFFERENCES ON NEUTRAL SURFACES

(i) Changes in salinity and temperature

Figure 3 shows the spatial distributions of changes in salinity on neutral surfaces, $S'|_n$, along the four zonal WOCE sections. The western and eastern boundaries have been excluded because the objective estimates tend to be unrealistic at the boundaries. The shaded parts denote areas where salinity has decreased over time. On a neutral surface, a change in salinity requires a compensating change in temperature. Hence the spatial distributions of changes in temperature on neutral surfaces $\theta'|_n$ are similar (with variations owing to the nonlinearity of the equation of state) to those in Fig. 3, and so are not shown. The right-hand panels in Fig. 3 show the zonally averaged differences $\overline{S'|_n}$. Their confidence intervals will be discussed in the next section.

Differences along each section have their own distinctive features. Along the WOCE P1 section at 47°N, above 27.4γ^n, a rough east–west trend can be seen, with the point of demarcation or zero crossing occurring at approximately 155°W (Fig. 3a). East of this longitude, water displays salinity and temperature increases on neutral surfaces, and to the west, decreases. The biggest differences occur at about 180°, between 26.5 and 27.0γ^n, which is the temperature minimum layer along 47°N (Talley et al. 1991). There, the salinity decrease exceeds 0.1, and the corresponding potential temperature decrease exceeds 1°C on neutral surfaces. Below 27.4γ^n, which at 47°N is about 600 dbar, S and θ show basinwide decreases on neutral surfaces. However, the averaged differences are less than 0.004 for S and less than 0.03°C for θ, and are within the expected range of possible systematic errors in salinity measurements due to different standard seawater batches (Mantyla and Reid 1983).

Differences in salinity on neutral surfaces along the WOCE P3 section at 24°N are dominated by mesoscale features, making it difficult to discern a coherent pattern of change. However, between 26.4 and 27.4γ^n, broad areas of salinity and temperature decreases dominate (Fig. 3b). This density range encompasses the intermediate salinity minimum of NPIW along 24°N (Roemmich et al. 1991), which is a water mass that acquires its properties from the subarctic North Pacific (Reid 1965). The maximum zonally averaged salinity decrease is 0.017 on the 27.0γ^n surface, which is the core density of the NPIW layer along 24°N. At 27.0γ^n, the meridional gradient of salinity along 24°N has been estimated from the historical data to be roughly 0.01 per 1° latitude, increasing southward. Hence the observed salinity

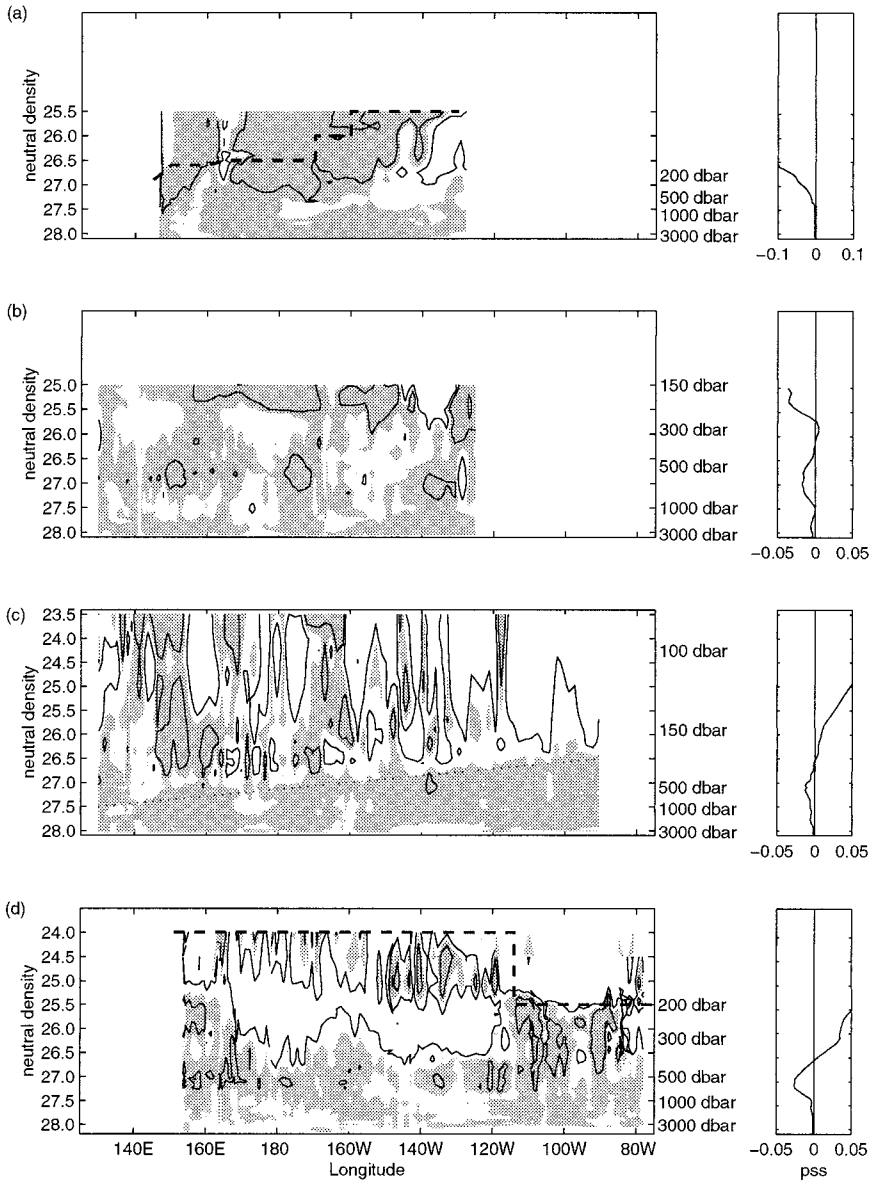

FIG. 3. Temporal differences of salinity on neutral surfaces $S'|_n$ along the four zonal WOCE sections: (a) P1 at 47°N, (b) P3 at 24°N, (c) P4 at 10°N, and (d) P21 at 17°S. All four profiles have been plotted on the same longitudinal and vertical axes. The shaded parts indicate areas with a salinity decrease on neutral surfaces. The isopleths mark $S'|_n = \pm 0.05$. The dashed lines mark the neutral surfaces above which the objective estimates are not reliable. The right-hand panels show the zonally averaged differences $\overline{S'|_n}$.

decrease on the $27.0\gamma^n$ surface along 24°N could be due to a less than 2° latitude, or roughly 200 km, southward excursion of the water mass. A southward excursion of the water mass will also be consistent with the observed deepening of the neutral surfaces (see next section). In the absence of other tracer data, such as oxygen or nutrients, it is difficult to determine whether the observed changes are due to lateral movements within the NPIW layer, or whether they represent real water mass property changes over time.

Along the WOCE P4 section at 10°N, at densities lighter than $26.5\gamma^n$, the water column displays extensive salinity and temperature increases on neutral surfaces to the east of 140°W (Fig. 3c). West of 140°W, the spatial picture is less coherent, but zonal averages taken between 130°E and 140°W show that between 24.0 and $25.5\gamma^n$, which encompasses a shallow salinity maximum, there has been significant mean temperature and salinity increases. This is North Pacific Subtropical Water (NPSTW; Wijffels et al. 1996), and has an origin under the subtropical evaporative cell. It is also present along the 24°N section, but its objective estimates at

24°N are not reliable and so its temporal changes at 24°N have not been discussed.

Below 27.0γ^n, all neutral surfaces along 10°N show basinwide decreases in S and θ. An intermediate salinity minimum is found in the density range 27.2–27.5γ^n (about 600–1000 dbar). This water mass is much denser than NPIW, and has been identified as a derivative of AAIW from the south (Wijffels et al. 1996). At densities greater than 27.9γ^n (below ≈2000 dbar), the averaged differences are less than 0.003 for salinity, and are indistinguishable from systematic salinity errors.

A feature worth noting along 10°N is that the spatial pattern of temporal change flips from basinwide salinity and temperature increases on neutral surfaces, to basinwide decreases, across a diagonal line that stretches from about 27.0γ^n at the western end of the transect, to about 26.5γ^n at the eastern end (marked by a dotted line in Fig. 3c). This diagonal line marks the position where the θ–S curve changes from a negative slope to a positive slope, around the intermediate salinity maximum along 10°N. This is a good illustration of the *pure warming* scenario of Bindoff and McDougall (1994), where a water mass that has experienced a temperature increase on isobars (see next section), actually displays different changes on isopycnals, depending on the slopes of its θ–S curve (Church et al. 1991). The salinity maximum shares similar θ–S characteristics to the 13°C thermostad in the eastern tropical Pacific, and Wijffels et al. (1996) have referred to it as 13°C Water.

Along the WOCE P21 section at 17°S, a large area stretching from roughly 170°E to 120°W shows salinity and temperature increases on neutral surfaces lighter than 26.5γ^n (Fig. 3d). These differences exceed 0.05 for S and 0.2°C for θ. A shallow salinity maximum, equivalent to NPSTW along 10°N, is present along 17°S at approximately 25.0γ^n (≈100 dbar), to the east of 160°W. Similar to NPSTW, this saline water mass is formed under the high evaporative cell of the South Pacific, and is naturally called South Pacific Subtropical Water (SPSTW).

At densities greater than 26.5γ^n, the temporal pattern of change along 17°S is dominated by basinwide decreases in S and θ. At the eastern half of the 17°S section, a shallow salinity minimum is found at about 26.5γ^n (≈300 dbar). It is formed near South America and is carried equatorward by the Peru–Chile Current. No thermostad (or pycnostad) associated with South Pacific STMW or SAMW is seen, as the WOCE P21 section lies north of the area where these two mode waters are found. However, a prominent salinity minimum layer is found between 27.0 and 27.5γ^n (about 400–1000 dbar) along the entire length of 17°S. The salinity minimum is associated with AAIW that has a core density of about 27.3γ^n. But the upper part of the salinity minimum layer includes densities that are lighter than the usual AAIW range (≈27.2–27.5γ^n), and is in fact in the SAMW range (≈27.0–27.1γ^n). Hence although no thermostad associated with SAMW is seen along 17°S, the thickness of the salinity minimum layer suggests that the water in the 27.0–27.1γ^n range (about 400–600 dbar) along 17°S is in fact an eroded version of SAMW. Zonally averaged differences show that the greatest salinity decrease in the SAMW–AAIW layer along 17°S is 0.026, found at 27.1γ^n.

Greater than 27.7γ^n along 17°S (below ≈1300 dbar), the salinity differences on neutral surfaces are less than 0.002 on average, within the systematic errors expected between the historical data and the modern CTD data. A set of deep western boundary currents are present in the subtropical southwest Pacific (e.g., Whitworth et al. 1999). At 17°S, the deep current is observed over the Tonga Trench east of the Tonga–Kermadec Ridge at about 172°W, which, at deeper than 4000 dbar, carries waters of Atlantic and Antarctic origins northward. Observation of a maximum chlorofluorocarbon signal at 5000 dbar indicates the strong Antarctic influence (Banks et al. 1995). It is in this region that variability could be expected (e.g., Johnson et al. 1994), but the sparse historical data around the bottom makes it difficult to detect any temporal changes with our method.

(ii) Changes in depths of neutral surfaces

Figure 4 shows the changes in depth of the neutral surfaces, N', along the four zonal WOCE sections. The shaded parts denote areas where isopycnals have deepened over time. The right-hand panels show the zonally averaged differences $\overline{N'}$. Along 47°N, neutral surfaces have mostly deepened east of 155°W, and have become shallower to the west (Fig. 4a). Isopycnals along 47°N slope downward from west to east in general, indicating broad interior northward flow relative to a deeper reference level across most the WOCE P1 47°N section. The observed temporal east–west change in neutral surface depths along 47°N means that the isopycnals are sloping downward more steeply from west to east in the 1980s than in the 1960s. This implies an increase in the northward transport across 47°N.

By the calculations of Roemmich and McCallister (1989), the flow across 47°N, excluding the western and eastern boundaries, is northward between 170°E and 140°W. To determine the change in transport due to the observed isopycnal heaving, volume transport has been calculated from the WOCE 1985 data, and from the objectively mapped historical data, for all station pairs from 170°E to 140°W, for the water column between 600 dbar (≈27.35γ^n) and 2000 dbar (≈27.90γ^n), with 2000 dbar being the reference level. According to the WOCE 1985 data, the total transport across 47°N between 170°E and 140°W is approximately 6 Sverdrups [$\equiv 10^6$ m^3 s^{-1} (Sv)] northward, between 600 and 2000 dbar. The total increase in northward transport within the same range is estimated to be 2.6 Sv, which represents a 76% increase from the 1960s to the 1980s. However, this estimation is sensitive to the choice of integration intervals. For example, if the integration in-

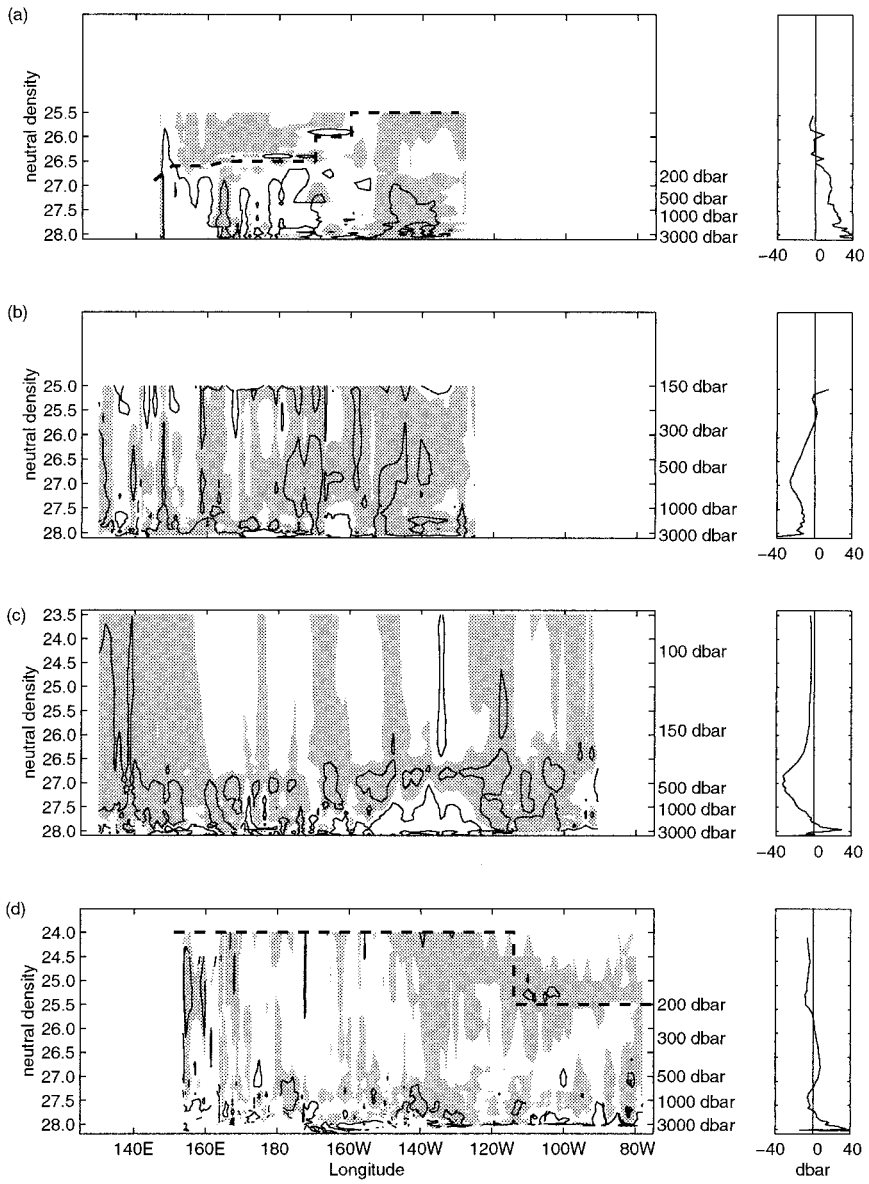

FIG. 4. Temporal differences of pressure of neutral surfaces N' (dbar) along the four zonal WOCE sections: (a) P1 at 47°N, (b) P3 at 24°N, (c) P4 at 10°N, and (d) P21 at 17°S. Negative values (shaded parts) indicate a deeper surface during the WOCE period. The isopleths mark $N' = \pm 40$ dbar. The right-hand panels show the zonally averaged differences $\overline{N'}$ (dbar).

tervals are expanded eastward and westward by 4° longitude (i.e., if transports are estimated between 166°E and 136°W), then the percentage increase in northward transport within the same depth range is only 43%. On the other hand, if the integration intervals are shortened eastward and westward by 4° longitude, the percentage increase is 80%.

Isopycnal movements along 24°N (Fig. 4b) are different from the changes along 47°N, in that no significant east–west variation has been observed, but all neutral surfaces from $25.7\gamma^n$ (≈270 dbar) to the deepest surface have become deeper on average along 24°N. There are examples of similar observations in the North Pacific that hint at a deepening of the subtropical gyre. For example, Watanabe and Mizuno (1994) found that the top 400 m between 10° and 25°N has warmed, while Shuto (1996) found that temperature to 1000 dbar along the 137°E meridian between 14° and 26°N was warmer from 1977 to 1985, than from 1970 to 1976. Our sectional averages show that temporal S and θ changes on neutral surfaces along 24°N are not statistically significant between $25.6\gamma^n$ (≈250 dbar) and $26.5\gamma^n$ (≈450 dbar). It is therefore likely that these changes in the temperature field, observed by Watanabe and Mizuno

(1994) and Shuto (1996), are caused by downward movements of the isotherms, and are not due to changes in the θ–S relationship of the water masses. Hence the distribution of these subsurface temperature anomalies may imply a deepening of the subtropical gyre after the mid-1970s.

Similar average deepening of isopycnals is also present along 10°N (Fig. 4c). Furthermore, Qiu and Joyce (1992) found that along the 137°E meridian, from 1967 to 1988, the transports of both the Kuroshio Current and the North Equatorial Current displayed a gradual increase, that is accompanied by a steady increase in magnitude of the North Pacific subtropical wind gyre. Our results of the general deepening of neutral surfaces along 24° and 10°N are consistent with the observations that the North Pacific subtropical gyre has been gradually deepening since the mid-1960s.

Along the WOCE section at 17°S, on the other hand, neutral surfaces lighter than $26.0\gamma^n$ have shown a slight zonal variation. Neutral surfaces have shoaled to the west of 140°W, and have deepened to the east of 140°W (Fig. 4d). This east–west variation might be an effect of the 1994 El Niño that resulted in an uplifting of the thermocline in the western Pacific, and eastward movements of warm water, causing a deepening of the thermocline in the eastern Pacific.

Between 26.0 and $27.0\gamma^n$ ($\approx$300–500 dbar), isopycnals along 17°S have shoaled in general. In the southwest Pacific west of 180°, between 10° and 30°S, Ridgway and Godfrey (1996) have observed cooling of the water column on isobars above 450 dbar (about $26.5\gamma^n$), between 1975–79 and 1985–89, and have interpreted this temperature decrease on isobars as due to a shallowing of thermocline waters. Holbrook and Bindoff (1997) also observed cooling of the water column above 450 dbar in the same region, since the mid-1970s, that has been accompanied by a decrease in steric sea level. By our observations along 17°S, the upward heave phenomenon observed previously in the southwest Pacific has continued to 1994, and extended down the water column to about 500 dbar along 17°S. No significant zonal variation in heave has been observed in this density range, implying that changes in the strength of the meridional transport at this level is negligible.

2) Differences on isobars

Salinity and temperature differences on isobars ($S'|_z$ and $\theta'|_z$) in the top 2000 dbar along the four zonal WOCE sections are shown in Figs. 5 and 6 respectively. The right-hand panels show the zonally averaged differences $\overline{S'_z}$ and $\overline{\theta'|_z}$. Only the top 2000 dbar are discussed because examination of differences on neutral surfaces shows that below 2000 dbar, changes to Pacific water properties are likely due to systematic errors between the WOCE and historical measurements (see previous section).

Along 47°N, cooling and freshening dominate the top 200 dbar, except for the small region east of 140°W, where warming on isobars can be seen (Fig. 6a). Below 200 dbar, general cooling is found between 200 and 1600 dbar to the west of 155°W, and is accompanied by salinity increase (Fig. 5a). To the east of 155°W below 200 dbar, warming has occurred and is accompanied by general freshening.

The east–west division in the temporal changes along 47°N is intriguing. Several features in the subarctic gyre might contribute to this division. For example, part of the westward-flowing Alaskan Stream branches off near 160°W, flowing southeastward and forming the cyclonic Alaskan gyre in the northeastern Pacific. The upper 250 m of the eastward-flowing Subarctic Current also branches off near 150°W: one branch turning north into the Gulf of Alaska, and one branch turning south into the California Current (Favorite et al. 1976). However, the east–west division extends below 500 dbar, deeper than these wind-driven features. Also, water at densities greater than $26.9\gamma^n$ (200–300 dbar) derives its properties from the Okhotsk Sea (Talley 1991), and so the east–west division at those densities could not be due to different sources.

A possible explanation for this east–west division lies in the year distribution of the historical data. Examination of the historical data north of 36°N shows that east of 155°W, the data are dominated by historical casts from 1957, while west of 155°W, the majority of the historical casts were sampled between 1966 and 1970. Hence the signatures to the east of 155°W are for a period that is 10 years longer than those to the west. The east–west division along 47°N therefore concurs with the SST map of Zhang and Levitus (1997) that shows, along 42.5°N, a positive anomaly west of 170°W during 1966–70, and a shift to a negative anomaly by 1980, suggestive of a cycle of temperature anomaly circulating around the North Pacific.

The spatial pattern of change along 24°N is less organized than along 47°N. However, at the intermediate salinity minimum of NPIW, which, at 24°N, stretches from about 400 dbar at the eastern end of the section, to about 700 dbar at the western end, there is basinwide freshening on isobars (Fig. 5b), and is accompanied by general warming (Fig. 6b). The corresponding changes on neutral surfaces are of basinwide decreases in salinity and temperature (see previous section). The changes observed in NPIW along 24°N therefore fit the *pure freshening* scenario of Bindoff and McDougall (1994), where freshening of a water mass leads to observed salinity decreases (and therefore θ decreases) on neutral surfaces.

Along 10°N, the spatial pattern of change on isobars is related to water mass distribution. Between 100 and 200 dbar, temporal changes west of 170°W are dominated by increase in salinity (Fig. 5c), and are accompanied by some warming. This is the area where the shallow salinity maximum of NPSTW is found. These observed changes are in accord with the *pure salination* scenario (Bindoff and McDougall 1994), where an increase in salinity of

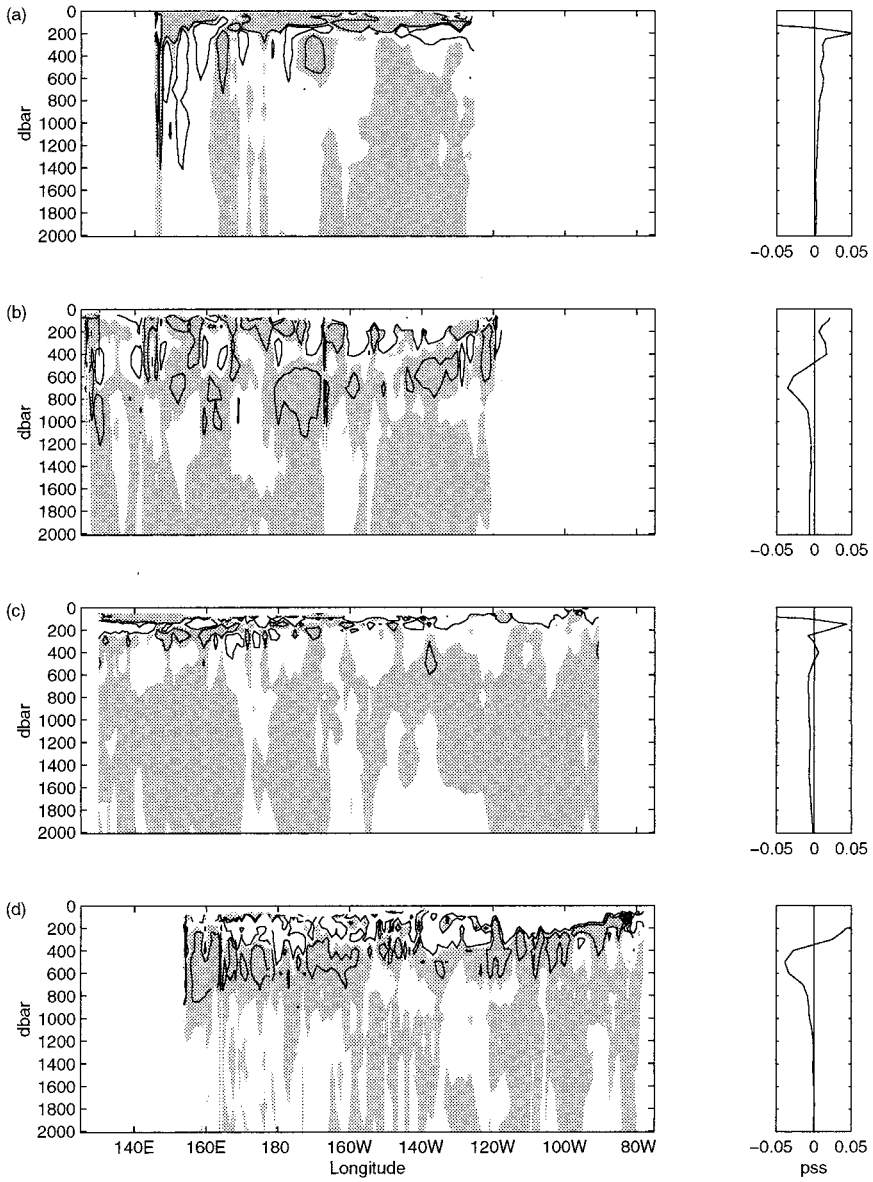

FIG. 5. Temporal differences of salinity on isobars $S'|_z$ for the upper 2000 dbar along the four zonal WOCE sections: (a) P1 at 47°N, (b) P3 at 24°N, (c) P4 at 10°N, and (d) P21 at 17°S. The shaded parts indicate areas that have experienced freshening on isobars. The isopleths mark $S'|_z = \pm 0.05$. The right-hand panels show the zonally averaged differences $\overline{S'|_z}$.

a water mass leads to a corresponding S increase (and therefore θ increase) on neutral surfaces.

Deeper in the water column between 200 and 600 dbar along 10°N, the water column shows warming as well as salinity increase on isobars. This depth range encompasses the entire layer of 13°C Water. As discussed in the previous section, S and θ changes on neutral surfaces in this depth range flips from basinwide increases, to decreases, across a diagonal line that marks the salinity maximum of 13°C Water. Combining the observed changes on neutral surfaces with warming on isobars, the differences in 13°C Water along 10°N therefore illustrates the *pure warming* scenario of Bindoff and McDougall (1994). Tsuchiya (1981) has traced the high salinity characteristic of 13°C Water to the Tasman Sea and northeast of New Zealand, between 35° and 40°S. However, Toggweiler et al. (1991) found Tsuchiya's (1981) origin for 13°C Water to be inconsistent with prebomb $\Delta^{14}C$ distribution in the Pacific, and proposed that it may originate as part of a single subduction process in the subantarctic region of the southwest Pacific. In any case, our observation implies surface warming in the southwest Pacific region. This agrees with Parker et al's (1994) surface temperature anomalies map for

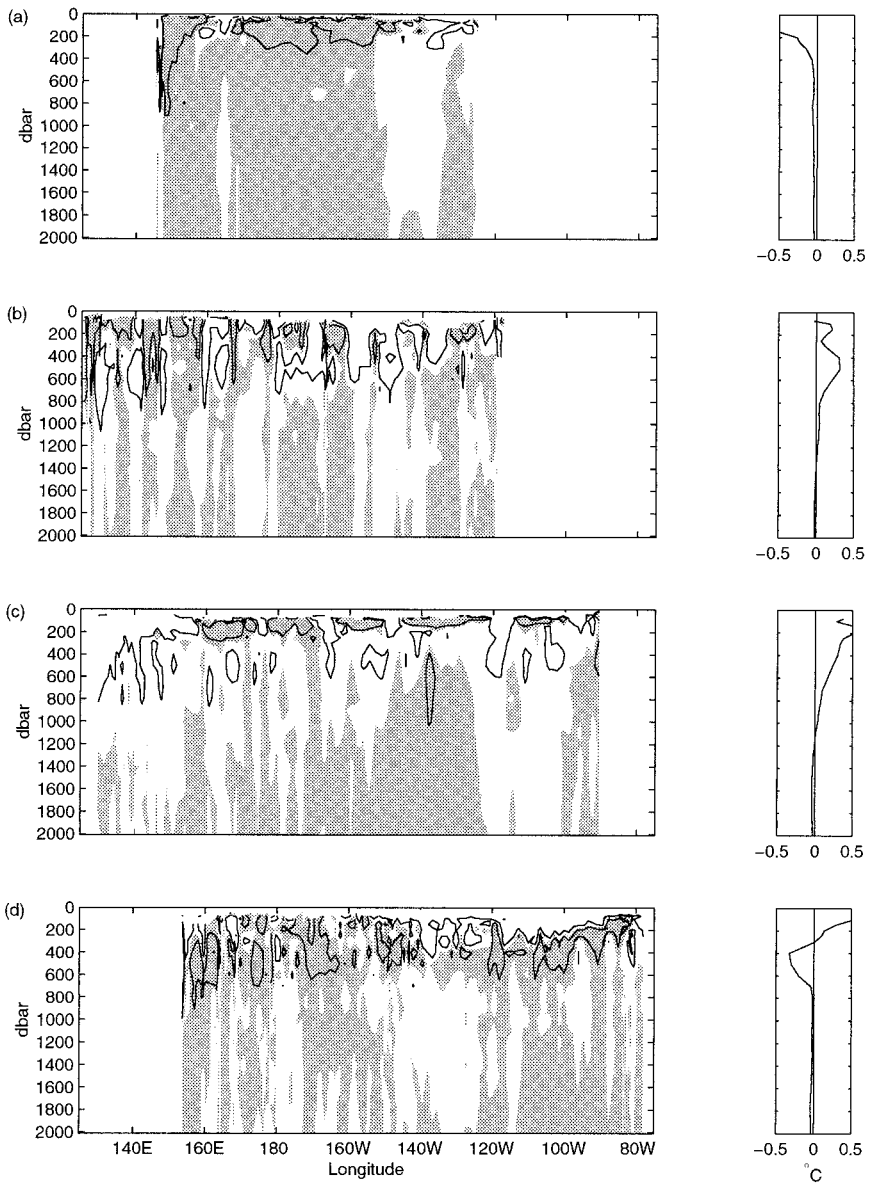

FIG. 6. Temporal differences of potential temperature on isobars $\theta'|_z$ (°C) for the upper 2000 dbar along the four zonal WOCE sections: (a) P1 at 47°N, (b) P3 at 24°N, (c) P4 at 10°N, and (d) P21 at 17°S. The shaded parts indicate areas that have experienced cooling on isobars. The isopleths mark $\theta'|_z = \pm 0.5$°C. The right-hand panels show the zonally averaged differences $\overline{\theta'|_z}$ (°C).

1981–90, relative to 1951–80, which shows positive anomalies over the southwest Pacific region. Holbrook and Bindoff (1997) also found long-term warming trend in the southwest Tasman Sea between 1955 and 1988.

Of the four zonal WOCE sections, P21 along 17°S is the only section that was carried out during an El Niño year (1994). As a consequence, temperature changes in the top 300 dbar of the water column along 17°S could be affected by the El Niño event. To the west of 140°W, cold anomalies dominate, while to the east of 140°W, warm anomalies are present (Fig. 6d). This east–west variation is not present in salinity differences in the top 300 dbar, where the majority of the water column shows salinity increases. In particular, the shallow salinity maximum along 17°S, SPSTW, has experienced salinity increases on isobars as well as on neutral surfaces. Hence, similar to its northern counterpart NPSTW, SPSTW has also undergone changes that are consistent with the *pure salination* scenario.

At about 300 dbar, the shallow salinity minimum at the eastern half of 17°S has shown freshening. Along both 10°N and 17°S, the AAIW layer (between 600 and

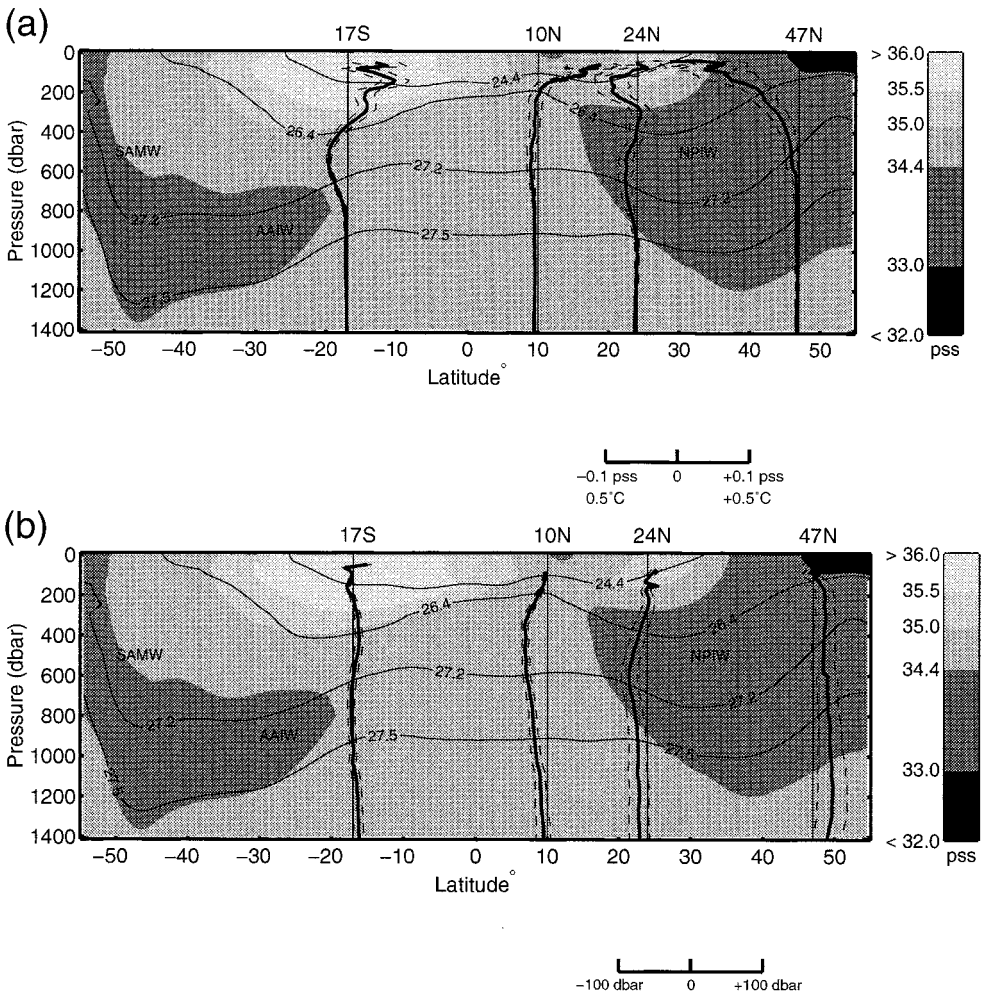

FIG. 7. Zonally averaged differences on neutral surfaces (solid lines) of (a) salinity $\overline{S'|_n}$, and (b) depth $\overline{N'}$ (dbar), along the four zonal WOCE sections at 47°N, 24°N, 10°N, and 17°S. These averaged differences are the same as in the right-hand panels of Figs. 3 and 4, but are plotted here on pressure coordinates. The dashed lines mark the 90% confidence intervals. The background is the salinity field along 160°W in the Pacific Ocean from the Levitus (1982) dataset. The approximate positions of the 24.4, 26.4, 27.2, and 27.5γ^n surfaces are superimposed. An approximate scale for $\overline{\theta'|_n}$ (°C) is provided in (a). Adapted from Wong et al. (1999).

1000 dbar), and the modified SAMW layer (400–600 dbar) along 17°S, have shown basinwide freshening (Figs. 5c,d). This is accompanied by warming along 10°N, but cooling along 17°S.

b. Zonally averaged temporal changes

1) DIFFERENCES ON NEUTRAL SURFACES

In order to filter out the mesoscale features and to examine the overall pattern of the observed temporal changes in the North and South Pacific Oceans, the differences on neutral surfaces have been averaged zonally along the four WOCE sections, and have been shown in the right-hand panels in Figs. 3 and 4. Figure 7 plots the same zonal averages: $\overline{S'|_n}$ (Fig. 3), and $\overline{N'}$ (Fig. 4), but in pressure coordinates, against a background of the climatological salinity field of the Pacific (Levitus 1982). The purpose is to show the magnitude and distribution of the temporal changes relative to the positions of the Pacific water masses. Only the upper 1400 dbar is shown because the changes there contain the most variations. The 90% confidence intervals, based on the T distribution, have been calculated for these zonal averages, and take into account the noise variance in the data that is caused by random processes such as mesoscale eddies and internal waves.

It can be seen that along all four sections, the water masses between 26.4 and 27.5γ^n have experienced salinity and temperature decreases on neutral surfaces that are above the 90% confidence levels. Within this density range are the salinity minima associated with NPIW (along 24°N), AAIW (along 10°N and 17°S), and modified SAMW (along 17°S). Examination of differences

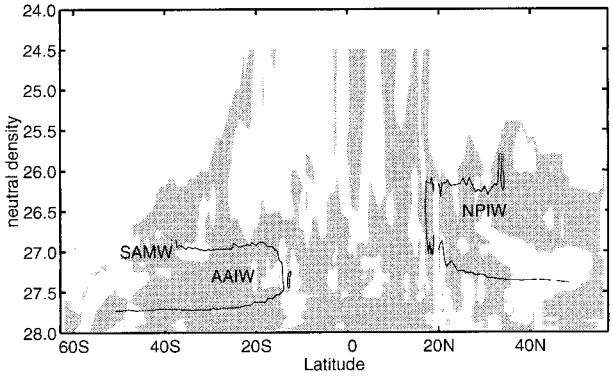

FIG. 8. Temporal differences of salinity on neutral surfaces $S'|_n$ along the meridional P16 WOCE section at 150°W. The shaded parts indicate areas with a salinity decrease on neutral surfaces. The two isopleths are $S = 34.2$, which marks the extent of NPIW, and $S = 34.5$, which marks the extent of AAIW. The approximate location of SAMW is also shown.

on isobars reveals that these S and θ decreases on neutral surfaces in the salinity minimum layers are accompanied by basinwide freshening on isobars (see previous sections). In the shallower layers above the salinity minimum where the $\theta-S$ slope is positive, a decrease in salinity on neutral surfaces can be caused by a combination of warming and freshening in the surface waters (Bindoff and McDougall 1994). However, at the salinity minimum, only freshening of the water mass can displace salinity toward lower values. Hence the observed salinity decrease in NPIW, AAIW, and modified SAMW, is most likely caused by freshening of surface waters in the source regions of NPIW and AAIW/SAMW (Wong et al. 1999).

Temporal differences have been examined along the meridional WOCE P16 section at 150°W to explore the extent of the freshening of NPIW and AAIW/SAMW. Figure 8 shows the salinity differences on neutral surfaces along 150°W, with the extents of NPIW and AAIW marked by the $S = 34.2$ and 34.5 isopleths, respectively. At the southern end of P16, the signature pycnostad of SAMW is found in the 27.0–27.1γ^n range, between 50° and 30°S, overlying the AAIW layer. AAIW along 150°W extends equatorward to about 10°S. It can be seen from Fig. 8 that salinity decreases on neutral surfaces dominate the SAMW and AAIW layers equatorward from the subantarctic front at about 52°S. In the North Pacific, NPIW along 150°W extends equatorward to about 15°N, and extensive salinity decreases on neutral surfaces are present. Averages taken between 50° and 10°S for AAIW, and between 15° and 50°N for NPIW, reveal that these salinity decreases on neutral surfaces are accompanied by freshening on isobars. These results therefore confirm the observed freshening of NPIW and AAIW through the centre of the subtropical gyres of the Pacific. In addition, SAMW has also undergone freshening.

NPIW is formed from mixing cold, fresh subpolar waters with warmer, more saline subtropical waters at the Oyashio–Kuroshio mixed water region (Talley 1993). The cold, fresh subpolar waters attain their characteristics in the subarctic gyre by general vertical diffusion (Reid 1965), and in the Okhotsk Sea through vertical mixing as a result of sea ice formation (Talley 1991; Warner et al. 1996). Numerous theories have been proposed on the formation of AAIW. Reid's (1965) study showed that some part of AAIW may derive its characteristics from the region between 55° and 65°S (approximately where the Polar Frontal Zone is in the South Pacific). McCartney (1977) has suggested that for the South Pacific variety of AAIW, the initial formation involves cooling and overturning of SAMW in the southeast Pacific. In short, both NPIW and the South Pacific variety of AAIW have their origins in the high latitudes of the North and South Pacific Oceans.

The observed freshening in NPIW and AAIW, and SAMW, therefore implies, to a first approximation, surface freshening over the high latitudes of the North and South Pacific Oceans. Unfortunately, no direct observations of decadal rainfall trends are available to verify the implied increase in high-latitude net precipitation. However, note that the averaged freshening of the AAIW layer along 10°N is half that along 17°S. For example, the maximum zonally averaged salinity decrease along 10°N is 0.01 at 27.2γ^n. At the same density, salinity decrease along 17°S is 0.02 (Fig. 7a). This is consistent with the first approximation that the changes originated from the AAIW formation region at the southern high latitudes, and have been lessened upon reaching 10°N by a combination of distance from the source and mixing.

Although a salinity minimum is not present in the subarctic waters along 47°N, freshening is also observed in water in the 25.5–26.0γ^n range. In the North Pacific, these density layers outcrop at a narrow zonal band along roughly 35°–40°N, and in the northeast Pacific, east of 160°W and north of 40°N. However, only the northeast Pacific has surface salinity less than 33. Because water in the 25.5–26.0γ^n density range along 47°N has salinity less than 33, it is concluded that this water has its origin in the Gulf of Alaska. The freshening observation in water of this density along 47°N therefore implies an increase in precipitation minus evaporation ($P - E$) rates over the northeastern Pacific. This implication is supported by observations of surface salinity trends from four ocean stations off the Pacific coast of Canada (including Ocean Station Papa; Freeland and Whitney 1997; Freeland et al. 1997).

In the shallower layers, salinity has increased on neutral surfaces and on isobars, to 25.5γ^n along 10°N, and to 26.2γ^n along 17°S. Within these shallow densities are NPSTW (along 10°N) and SPSTW (along 17°S), which are two saline water masses that originate under the high evaporative cells in the subtropical North and South Pacific, and are subducted into the thermocline and advected equatorward. These salinity increases therefore

imply a decrease in $P - E$ rates over the Pacific subtropical gyres. Note that Kessler (1999) has also observed a general rise in salinity in the high salinity tongue on 24.5 σ_t during the 1990s, between 10°N and 10°S, along 165°E, 180°, and 155°W. However, the inferred subducted variability from the ventilation region was found to be inconsistent with the observed downstream salinity changes.

In general, the results from the North Pacific Ocean agree with those from Antonov (1993), that deeper than 600 m, temperature changes in the North Pacific from 25° to 60°N are negligibly small. Along the WOCE section at 47°N, temperature and salinity changes are only significant at the 90% confidence levels to about 530 dbar. This lack of deep water property changes reflects the lack of formation, and hence ventilation, of deep waters in the North Pacific, relative to the North Atlantic.

Equatorward of 25°N, temperature and salinity changes have been observed at greater depths. For example, along the WOCE section at 24°N, changes are significant at the 90% confidence levels to about 1000 dbar. Along 10°N and 17°S, changes are significant at the 90% confidence levels to about 2000 and 1300 dbar, respectively, and reflect the influence on the deeper waters of the equatorial and South Pacific from the Southern Ocean. Below 2000 dbar, no statistically significant water property changes has been observed in the North and South Pacific.

2) Differences on isobars

Along a hydrographic section from cast_a to cast_b, changes in salinity and potential temperature on isobars can be integrated zonally for each neutral density layer as follows:

$$\Delta s_i = \int_{\gamma_i^n}^{\gamma_{i+1}^n} \int_{\text{cast}_a}^{\text{cast}_b} S'|_z \, dl \, dz_\gamma$$

$$\Delta \theta_i = \int_{\gamma_i^n}^{\gamma_{i+1}^n} \int_{\text{cast}_a}^{\text{cast}_b} \theta'|_z \, dl \, dz_\gamma, \qquad (1)$$

where l (in meters) is the horizontal distance between casts along the hydrographic section, z_γ (in meters) is the vertical distance between the two neutral surfaces. The advantage of integrating temporal changes in this manner is that the vertical distribution of Δs_i and $\Delta \theta_i$ can be examined to show which neutral density layer contributes more to the overall salinity and potential temperature changes. Here $S'|_z$ and $\theta'|_z$ are the temporal changes on isobars, in salinity and potential temperature respectively, at the time-average depths of respective neutral surfaces at each cast. The Δs_i and $\Delta \theta_i$ therefore are the area-weighted and zonally integrated isobaric changes for each neutral density layer γ_i^n to γ_{i+1}^n, and have units m^2 and °C m^2, respectively. They are therefore different from the zonal averages of $\overline{S'|_z}$ and $\overline{\theta'|_z}$ (°C), which are shown in the right-hand panels of Figs. 5 and 6. Note that because differences on isobars are used, Δs_i and $\Delta \theta_i$ combine water mass changes and effects of vertical movements of isopycnals.

Here Δs_i and $\Delta \theta_i$ have been calculated for all the neutral density layers along the four zonal WOCE sections, excluding the western and eastern boundaries, and are shown in Figs. 9 and 10, respectively. Note that the upper- and lower-limit γ^n levels are different between the four sections. The upper-limit γ^n levels have been chosen to exclude the highly variable surface mixed layer where objective estimates are unrealistic. The lower-limit γ^n levels represent the deepest surface below which temporal differences cannot be separated from instrumental errors.

It can be seen from Fig. 9, that along all four sections, a clear change in Δs_i occurs in the 26.3–27.0γ^n range. This corresponds to a change in regime in the distribution of the thermohaline properties. Along 47°N, the change occurs at the base of the thermocline, at about 165 dbar (26.75γ^n). Below the thermocline, upward displacements of isopycnals contribute to increases in salinity. Along 24°N, 10°N, and 17°S, where an intermediate salinity minimum associated with either NPIW or AAIW/SAMW exists, the change in sign of Δs_i occurs in the transition zone between salty upper waters and low-salinity intermediate waters. This transition zone is at about 500 dbar along 24°N (26.65γ^n) and 10°N (27.05 γ^n), and at about 300 dbar along 17°S (26.3γ^n). The upper waters give an overall salinity increase and the waters below give an overall reduction in salinity. However, the salinity increases in the upper waters are less than the salinity decreases in the intermediate and deep waters. It is estimated that the salinity increases in the upper layers balance the salinity decreases in the deeper layers by 60% along 24°N, by 56% along 10°N, and by only 29% along 17°S. Because the salinity decreases in the intermediate and deeper waters are only partially balanced by the salinity increases in the upper waters, overall these three sections have experienced a small increase in freshwater input (see next section).

Unlike changes in salinity, where the upper waters exhibit changes that are different from the intermediate layers, the distribution of temperature changes shows no such vertical features. In fact, the vertical distribution is almost monotonic with depth. In the subarctic Pacific, the entire water column has cooled along 47°N, with the biggest temperature decrease being through the shallower layers, and lesser through the deeper levels (Fig. 10a). On the other hand, in the subtropical and tropical North Pacific, the water column down to 27.5γ^n (≈1000 dbar) has warmed. Along 24°N, the largest temperature increase is at the 26.5γ^n level, while along 10°N, the largest temperature increase is at the 27.0γ^n level (Figs. 10b,c). These are the upper density ranges of NPIW and modified AAIW, respectively, and are both at about 500 dbar.

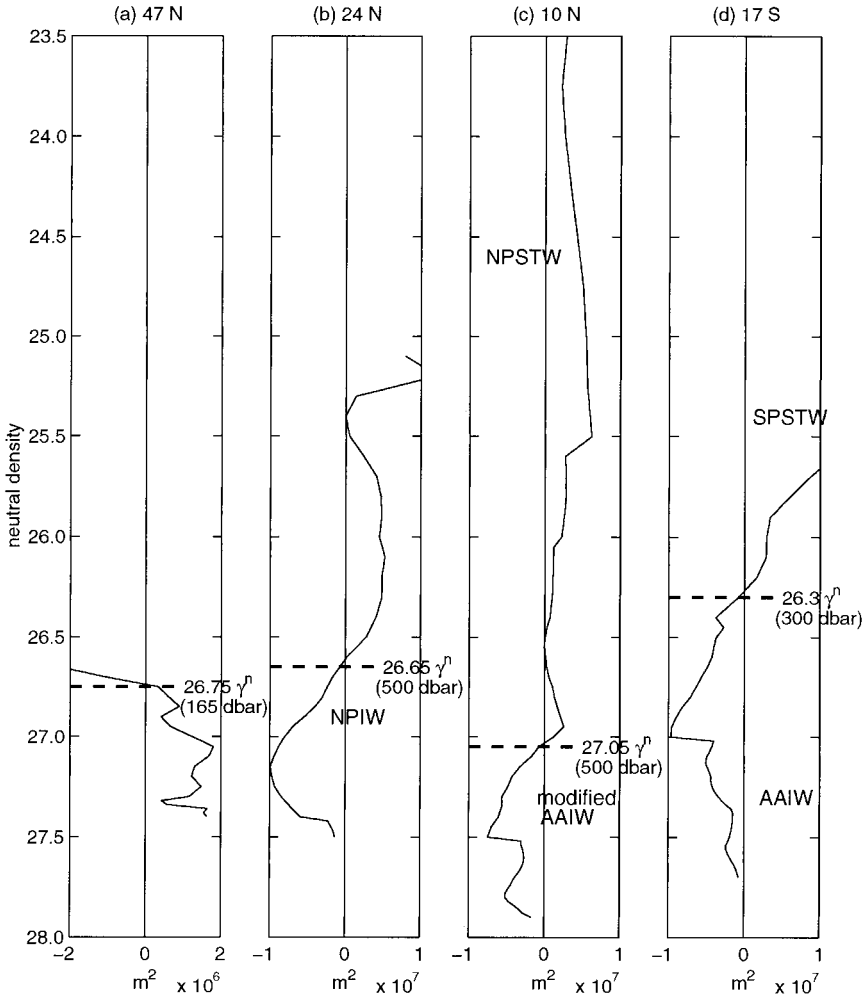

FIG. 9. The distribution of the area-weighted and zonally integrated salinity change Δs_i (m^2) for each neutral density layer, along the four zonal WOCE sections. Note that the scale for (a) is different from (b), (c), and (d). The dashed lines mark the density (and approximate pressure) where Δs_i changes from positive to negative.

For comparison, in the North Atlantic along 24°N, the maximum warming has been observed from about 1100 down to 2000 dbar (Bryden et al. 1996). Similarly, the time series at Bermuda (≈32°N) shows long-term warming in the deeper waters between 1500 and 2500 dbar (Joyce and Robbins 1996). Recent findings by Joyce et al. (1999) have shown that the western part of the North Atlantic subtropical gyre between 20° and 35°N have experienced significant warming between 800 and 2500 m from 1954–58 to 1997. Thus, relative to the subtropical North Atlantic, the subtropical North Pacific has warmed to shallower depths.

Within the North Pacific itself, the opposite trends in temperature change that have been observed between the subarctic (47°N) and the subtropical (24° and 10°N) gyres are in agreement with other studies on decadal variability in the ocean interior. For example, Zhang and Levitus (1997) revealed a subsurface (250 m) thermal anomaly that circulates around the North Pacific in a clockwise manner, and could account for the observed opposite trends. Levitus et al. (1994) have also shown a quasi-decadal oscillation in the temperature anomaly field at 125 m in the North Atlantic Ocean.

In the South Pacific, the WOCE section at 17°S behaves differently from the other three zonal sections in the North Pacific, in that there is a change of sign in the vertical temperature change profile. Above $26.0\gamma^n$, the water column has warmed; below $26.0\gamma^n$, the water column has mostly cooled (Fig. 10d). The biggest temperature decrease is near the $27.0\gamma^n$ level, which is in the modified SAMW density range.

In the next sections, these temporal differences in salinity and temperature on isobars are integrated to estimate changes in freshwater and heat contents, and finally changes to the steric sea level, in the Pacific Ocean over the 20-yr study period.

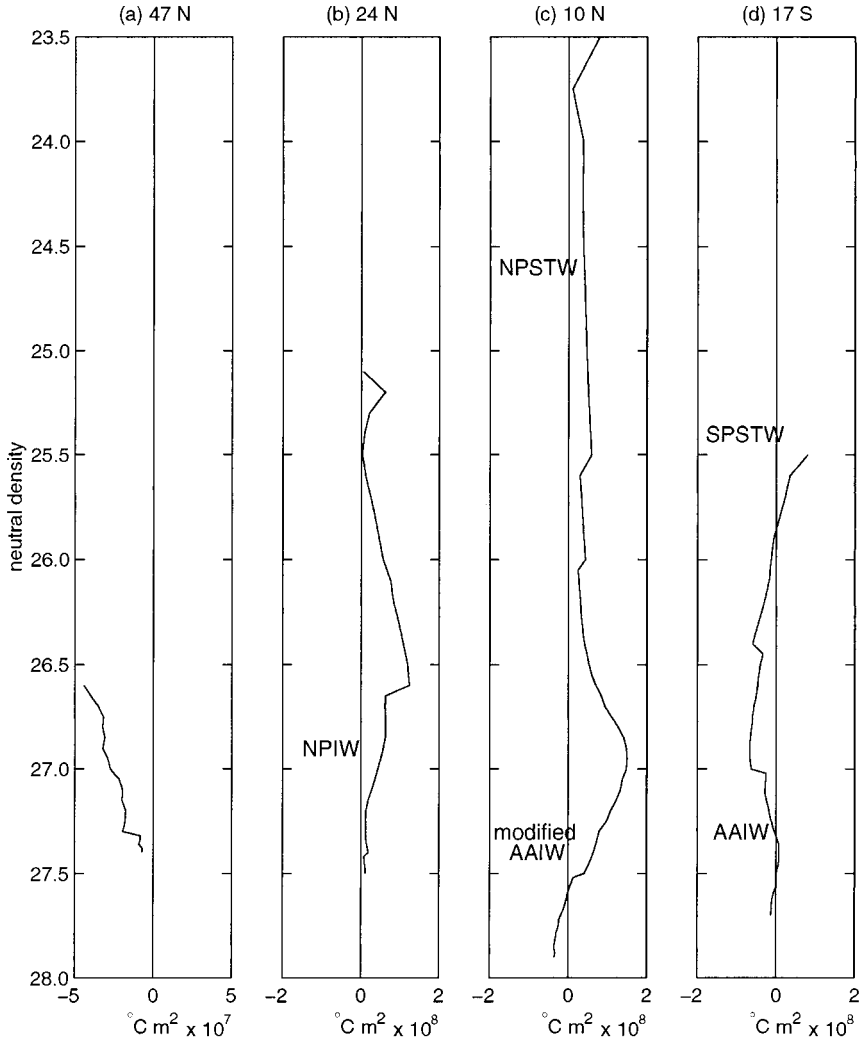

FIG. 10. The distribution of the area-weighted and zonally integrated potential temperature change $\Delta\theta_i$ (°C m²) for each neutral density layer, along the four zonal WOCE sections. Note that the scale for (a) is different from (b), (c), and (d).

4. Changes in freshwater and heat contents

a. Freshwater content change

Since salt is conserved in the ocean, changes in salinity are the result of addition or removal of freshwater to or from the ocean. For a column of water with 1-m² cross-sectional area and H m in depth, changes in its freshwater content and its salinity have the relation

$$H\overline{S} = (H + \Delta f)(\overline{S} + \overline{\Delta s}), \tag{2}$$

where H (in meters) is the depth of the water column, $\overline{S}$ is the average salinity of the water column, Δf (in meters) is the change in height of the water column due to addition or removal of freshwater. Here $\overline{\Delta s}$ is the depth-integrated change in salinity of the water column bounded by two neutral surfaces γ_x^n and γ_y^n, and is calculated from the sectional area-weighted change Δs_i from Eq. (1) by

$$\overline{\Delta s} = \frac{1}{\iint dz_\gamma\, dl} \sum_{i=x}^{y-1} \Delta s_i.$$

Upon expansion, Eq. (2) becomes

$$\Delta f\overline{S} + H\overline{\Delta s} + \Delta f\overline{\Delta s} = 0.$$

Because the last term $\Delta f\overline{\Delta s}$ is small relative to the other two terms, to first-order accuracy, this equation can be written as

$$\Delta f = -\frac{H\overline{\Delta s}}{\overline{S}}. \tag{3}$$

A positive Δf indicates an increase in height of the water column due to addition of freshwater, and results in a negative $\overline{\Delta s}$, indicating a resultant decrease in salinity.

The depth-integrated salinity change $\overline{\Delta s}$ along the

four zonal WOCE sections, and the inferred amount of freshwater input/output Δf, are listed in Table 1. The upper-limit γ_y^n and the lower-limit γ_x^n are the same as those used in Fig. 9. Along the three sections with an intermediate salinity minimum associated with either NPIW or AAIW/SAMW, the overall salinity change $\overline{\Delta s}$ is a net decrease: 0.0049 along 24°N, 0.0016 along 10°N, and 0.0068 along 17°S. Along 47°N, the only WOCE section in this study that does not exhibit a distinct salinity minimum, the entire water column below $26.75\gamma^n$ gives a sectional area-weighted increase in salinity (see Fig. 9) that is more the result of upward displacement of isopycnals, resulting in a net salinity increase of 0.0038 (Table 1). Most of these net results are close to instrumental precisions for salinity observations.

The net salinity decreases along the three sections 24°N, 10°N, and 17°S are the result of salinity reductions in the intermediate and deep waters outweighing salinity increases in the upper waters. By integrating the upper waters separately from the intermediate and deep waters, the inferred freshwater losses by the upper waters are estimated to be 14.24 cm along 24°N, 12.49 cm along 10°N, and 9.6 cm along 17°S. On the other hand, the inferred freshwater gains by the intermediate and deep waters are 24.19 cm along 24°N, 20.77 cm along 10°N, and 28.67 cm along 17°S (Table 1). The inferred freshwater loss therefore balances the inferred freshwater gain by 29%–60% along these three sections, thus giving these three sections an overall increase in freshwater input (see Δf in Table 1).

The combined observations along 24°N, 10°N, and 17°S, of salinity increase in the upper waters and salinity decrease in the intermediate and deeper waters, are interesting. Most of the water masses in the upper layers along these three sections have a subtropical origin, while those in the intermediate and deep layers acquire their properties near the subpolar gyres. Extrapolating the salinity changes along these three sections to the rest of the Pacific implies a decrease in $P - E$ rates over the subtropics, and an increase in $P - E$ rates over the polar gyres. The combined observations therefore suggest a strengthening of the atmospheric hydrological cycle over the Pacific between the historical and WOCE periods (Wong et al. 1999). Hence although the overall depth-integrated salinity changes detected in the Pacific are small, there has been significant regional redistribution of freshwater that is associated with the water mass changes, and hence implies significant redistribution of surface freshwater fluxes over the Pacific.

b. Heat content change

Unlike the salt content of the global ocean, which is a conserved quantity, ocean temperature, or its heat content, is not conserved. The heat content change ΔQ of a parcel of water that has undergone an average temperature change of $\overline{\Delta\theta}$ is

$$\Delta Q = V\rho C_p \overline{\Delta\theta},$$

where V (m^3) is the volume of the parcel of water, ρ (kg m^{-3}) is the density of the parcel of water, and C_p (J K^{-1} kg^{-1}) is the specific heat of the water parcel at constant pressure p. The resulting heat content change ΔQ has units of J (Joules). The $\overline{\Delta\theta}$ is the depth-integrated change in potential temperature of the water column bounded by two neutral surfaces, γ_x^n and γ_y^n, and is calculated from the sectional area-weighted change $\Delta\theta_i$ from Eq. (1) by

$$\overline{\Delta\theta} = \frac{1}{\iint dz_\gamma\, dl} \sum_{i=x}^{y-1} \Delta\theta_i.$$

The resultant heat content change ΔQ is then given by

$$\Delta Q = \rho C_p \overline{\Delta\theta} H, \tag{4}$$

where H (m) is the averge depth of the water column, as in Eq. (3), and ΔQ has units in J m^{-2}.

Table 2 lists the depth-integrated potential temperature change $\overline{\Delta\theta}$, and the resultant heat content change ΔQ, along the four zonal WOCE sections. The upper and lower γ^n limits for integration are the same as those used in Fig. 1. The specific heat of a water parcel is a function of pressure, temperature, and salinity (Gill 1982). Here, C_p is taken to be 3.99×10^3 J K^{-1} kg^{-1}, which is the specific heat of seawater with $S = 35$ at surface pressure. Other C_p values are within $\pm 0.2 \times 10^3$ of this value. Here ρ is taken to be 1028 kg m^{-3} as the average density of seawater.

The largest depth-integrated temperature change $\overline{\Delta\theta}$ is 0.1701°C over 15 yr (0.007°C yr^{-1}) along 24°N (≈1970–85), between 160 and 990 dbar. This is larger than the deep observations in the North Atlantic of 0.1°C per 25 yr (0.004°C yr^{-1}), between 800 and 2500 m (1957–81; Antonov 1993), and of 0.57°C per century (0.0057°C yr^{-1}) in the western North Atlantic between 800 and 2500 m (1954–58 to 1997; Joyce et al. 1999). The resulting rate of heat content change of 1.1082 W m^{-2} along 24°N is comparable with estimates from coupled climate models of oceanic heat flux for doubling of atmospheric CO_2 along similar latitudes averaged around the globe (about 1.33 W m^{-2} from Manabe et al. 1990). Comparatively, between 1500 and 2500 dbar at Bermuda (32.17°N, 64.50°W), the rate of temperature rise amounts to 0.7 W m^{-2} (Joyce and Robbins 1996).

Over the study period, along 47°N and 17°S, the ocean has lost heat that amounts to 2.55×10^8 J m^{-2} and 2.23×10^8 J m^{-2}, respectively, while along 24° and 10°N, the ocean has gained heat of the amounts 4.82×10^8 J m^{-2} and 6.73×10^8 J m^{-2}, respectively. Based on these four sections, the overall heat content change in the Pacific between 60°N and 31.5°S is estimated to be a net gain of 1.79×10^8 J m^{-2} over the study period.

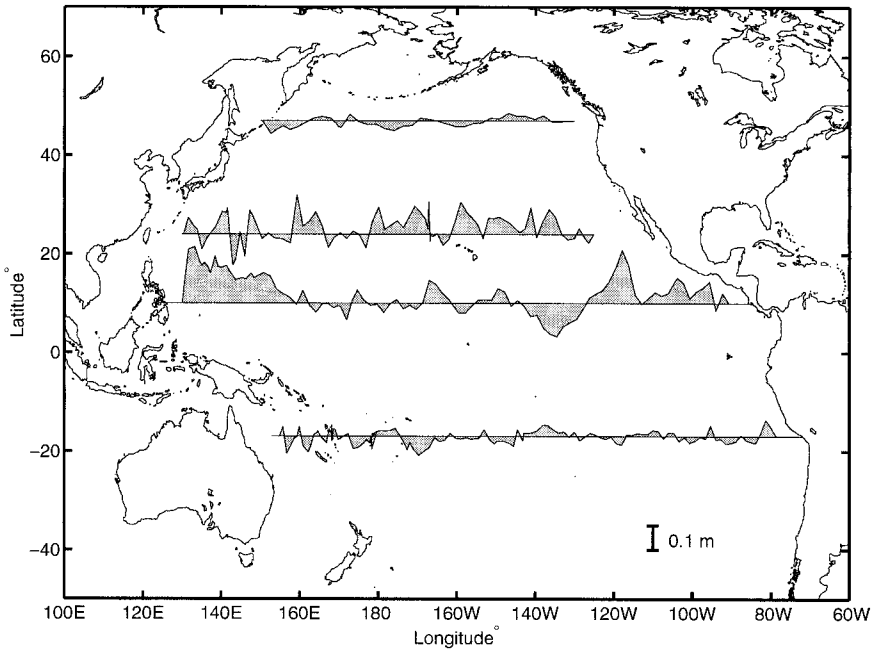

FIG. 11. Steric height change Δh (m) along the four zonal WOCE sections. The depth ranges of integration are shown in Table 3. Positive Δh means that sea level has risen.

5. Steric sea level change

The halosteric and thermosteric changes discussed in the previous sections combine to give a total steric height change estimate between the WOCE period and the historical data period. To calculate the steric height change, or sea level change, as a result of the observed temporal temperature and salinity differences ($\theta'|_z$ and $S'|_z$), the Equation of State for seawater in the form $\Delta\rho/\rho = \beta S'|_z - \alpha\theta'|_z$ is used. The depth-integrated steric height change Δh (in meters) is calculated as

$$\Delta h = \int_{\gamma_x^n}^{\gamma_y^n} \Delta\rho/\rho \, dz_\gamma = \int_{\gamma_x^n}^{\gamma_y^n} \beta S'|_z - \alpha\theta'|_z \, dz_\gamma$$
$$= \int_{\gamma_x^n}^{\gamma_y^n} \beta S'|_z \, dz_\gamma - \int_{\gamma_x^n}^{\gamma_y^n} \alpha\theta'|_z \, dz_\gamma. \quad (5)$$

Figure 11 shows the profile of sea level change Δh along the four zonal WOCE sections. Positive Δh means that sea level has risen. The vertical distributions of the halosteric and thermosteric contributions are similar to Figs. 9 and 10, and so are not shown. The steric height change is due to vertical isopycnal movements, that are the result of water mass property changes and vertical heave (without water mass changes). The limits of integration are the same as those used in Tables 1 and 2, and are listed in Table 3. It should be stressed again that the changes have been integrated over different parts of the water column along different sections, depending on the reliability of the objective estimates.

The largest amplitudes of sea level change occur along 10°N (−15 to 31 cm, relative to about 1950 dbar), and the smallest occur along 47°N (−5 to 4 cm, relative to about 650 dbar). In particular, along 47°N and east of 153°W, sea level has risen in the order of 1 mm yr^{-1} (relative to 650 dbar) between the WOCE period and

TABLE 1. Depth-integrated salinity change $\overline{\Delta s}$, and the inferred freshwater input/output Δf, along the four zonal WOCE sections. The separations between the upper and deeper layers are marked in Fig. 9. Negative Δs indicates an overall decrease in salinity, and the inferred Δf will be positive, indicating freshwater input into the section.

	P1 at 47°N	P3 at 24°N	P4 at 10°N	P21 at 17°S
Upper layer $\overline{\Delta s}$	−0.0483	0.0174	0.0124	0.0368
Upper layer Δf (cm)	2.64	−14.24	−12.49	−9.6
Deeper layer Δs	0.0066	−0.0209	−0.0052	−0.0115
Deeper layer Δf (cm)	−7.42	24.19	20.77	28.67
Total $\overline{\Delta s}$	0.0038	−0.0049	−0.0016	−0.0068
Total Δf (cm)	−4.8	10.0	8.3	19.1
Average years between WOCE and historical data Δt (yr)	19	15	20	27
Total $\Delta f/\Delta t$ (cm yr^{-1})	−0.25	0.66	0.42	0.71

TABLE 2. Depth-integrated temperature change $\overline{\Delta\theta}$, and the resultant heat content change ΔQ, along the four zonal WOCE sections. Positive $\overline{\Delta\theta}$ indicates an overall increase in potential temperature, and results in a positive ΔQ, indicating heat gain by the section.

	P1 at 47°N	P3 at 24°N	P4 at 10°N	P21 at 17°S
$\overline{\Delta\theta}$ (K or °C)	−0.1475	0.1701	0.0930	−0.0558
ΔQ ($\times 10^8$ Jm^{-2})	−2.55	4.82	6.73	−2.23
$\Delta Q/\Delta t$ (Wm^{-2})	−0.4253	1.0182	1.0663	−0.2617

the historical data period. This estimate is consistent with steric height trends relative to 1000 dbar in the northeast Pacific Ocean, measured at Ocean Station Papa at 50°N, 145°W (Thomson and Tabata 1987). At about 130°W along 24°N, sea level has also risen in the order of 1 mm yr^{-1} (relative to 990 dbar), which is consistent with observations along the southwest U.S. coast by Roemmich (1992).

Table 3 lists the average steric height change along each of the four zonal WOCE sections, and the respective thermosteric and halosteric components. It is obvious that in the open ocean away from coastal processes, thermosteric effect dominates the total steric height change. In particular, the thermosteric component accounts for 85%–94% of the sea level rise along 24° and 10°N.

The average steric sea level increases along 24° and 10°N far outweigh the average sea level decreases along 47°N and 17°S. Overall, the area-weighted steric height change for the North and South Pacific Oceans from 60°N to 31.5°S, based on the four zonal sections, is estimated to be a rise of 0.85 mm yr^{-1}. That is, because of significant ocean warming from the subtropical North Pacific, the overall steric sea level in the Pacific has risen in the roughly 20-yr period between the 1960s and 1985–94.

Studies from other regions have also quoted similar sea level rise estimates. For example, in the Tasman Sea, Bindoff and Church (1992) estimated a steric sea level increase of 2–3 mm yr^{-1} over 22 yr. In the western subtropical North Atlantic, Joyce et al. (1999) estimated a steric sea level rise of 1 mm yr^{-1} in the 40 yr between 1954–58 and 1997. In the Indian Ocean along 32°S, Bindoff and McDougall (2000) estimated a rise of 1.6 mm yr^{-1} over 25 yr. On a global scale, Douglas (1991) has obtained a mean sea level rise value of 1.8 ± 0.1 mm yr^{-1} over 76 yr, based on tide gauge records.

In the Intergovernmental Panel on Climate Change (IPCC) Second Assessment Report, contribution from thermal expansion to sea level rise over the the last 100 years based on model simulations is estimated to be in the range 0.2–0.7 mm yr^{-1} (p. 380, IPCC 1995). Thus, these ocean observations are beginning to reveal increases in sea level due to thermal expansion that are larger than that estimated by numerical models in the IPCC Second Assessment Report. There is a possibility that the lower rates of sea level rise estimated by the models are a result of the longer time span used in the averaging than most observational studies. In other words, these observational studies may be reflecting an increase in the rate of thermal expansion in recent decades. Also, observations contain more natural variability than in the models. Results such as those presented in this study are therefore important in providing observational evidence to test the effectiveness of numerical models in simulating the climate system. Such rigor is essential for accurate projection of global climate conditions under an enhanced greenhouse effect.

6. Discussion and conclusions

In this study, by comparing five modern CTD sections with historical hydrographic data, statistically significant changes in salinity and temperature have been detected in water masses that occur in the upper 2000 dbar of the water column in the North and South Pacific Oceans. Isopycnal depths have also changed, indicating an increase in northward transport across 47°N, a deepening of the North Pacific subtropical gyre, and a shallowing of thermocline waters along 17°S, over the study period.

At the same time, water properties of the deep Pacific below 2000 dbar remain essentially constant, or beyond instrumental detection, in accord with the long time-

TABLE 3. Average steric height change along the four zonal WOCE sections, and the respective thermosteric ($-\int \alpha\theta'|_z dz_\gamma$) and halosteric ($\int \beta S'|_z dz_\gamma$) components. The errors represent the 90% confidence intervals.

	P1 at 47°N	P3 at 24°N	P4 at 10°N	P21 at 17°S
Average steric sea level change $\overline{\Delta h}$ (mm)	−9.4 ± 1.79	26.6 ± 4.78	41.8 ± 2.68	−4.2 ± 1.69
Thermosteric component (mm)	−7.7	22.5	39.4	−9.9
Halosteric component (mm)	−1.7	4.1	2.4	5.7
% steric sea level change*				
Due to $\alpha\theta'|_z$	82%	85%	94%	63%
Due to $\beta S'|_z$	18%	15%	6%	37%
$\overline{\Delta h}/\Delta t$ (mm/yr)	−0.49 ± 0.09	1.77 ± 0.32	2.09 ± 0.13	−0.15 ± 0.06
Upper limit γ^n for integration	26.6 γ^n	25.1 γ^n	23.5 γ^n	25.5 γ^n
(approx pressure)	(130 dbar)	(160 dbar)	(85 dbar)	(200 dbar)
Lower limit γ^n for integration	27.4 γ^n	27.5 γ^n	27.9 γ^n	27.7 γ^n
(approx pressure)	(650 dbar)	(990 dbar)	(1950 dbar)	(1290 dbar)

* % steric sea level change due to $\alpha\theta'|_z$ is calculate as $|\alpha\theta'|_z|/(|\alpha\theta'|_z| + |\beta S'|_z|)$. Similarly for % steric sea level change due to $\beta S'|_z$.

scales required for ventilating waters below 2000 dbar in the Pacific Ocean, when compared with the relatively short average time difference of roughly 20 yr between the historical data and the WOCE sampling. In the abyssal subtropical southwest Pacific (below 3000 dbar), where deep western boundary currents provide more recently ventilated waters of North Atlantic and Antarctic origins, variability in North Atlantic Deep Water and Antarctic Bottom Water have been observed by comparing repeated full-depth high quality hydrographic sections (Johnson et al. 1994; Johnson and Orsi 1997). However, the sparse historical data around the bottom makes it difficult to detect any temporal changes in the abyssal layers in those regions by our method.

Comparatively, sea surface conditions in the North Atlantic are able to translate to greater depths than in the North Pacific, due to the stronger vertical convective activities in the North Atlantic. The North Atlantic vertical overturning cell reaches abyssal depths via the formation of North Atlantic Deep Water, and changes to Labrador Sea Water (LSW) have been observed at 2000 dbar. In the North Pacific, the upper vertical overturning cell that involves mode water and intermediate water is not deep reaching, and is essentially decoupled from the deep and abyssal vertical circulation of Circumpolar Deep Water and North Pacific Deep Water (e.g., Schmitz 1996; Sloyan and Rintoul 2001). Thus, relative to the subtropical North Atlantic, the subtropical North Pacific has experienced changes to shallower depths.

The freshwater and heat storage changes inferred from the observations give an indication of how the two main oceanic variables, salinity and temperature, change differently over time in the Pacific Ocean. Salinity changes are more related to the distribution of water mass properties, and although the net freshwater storage changes are small, the implied regional redistribution of surface freshwater fluxes at the formation regions of the various subtropical and intermediate water masses is significant. On the other hand, the heat storage changes are not as sensitive to water mass distributions. Significant warming in the subtropical North Pacific has caused a steric sea level rise of 0.85 mm yr^{-1} in the Pacific Ocean between 60°N and 31.5°S over the roughly 20-yr study period.

The freshening of Antarctic Intermediate Water (AAIW) in the Pacific Ocean observed by Wong et al. (1999) along 10°N and 17°S is here shown to extend southward to the Subantarctic Front in the South Pacific along 150°W, and includes Subantarctic Mode Water (SAMW) at the southern portion of the 150°W section. North Pacific Intermediate Water (NPIW) along 150°W has also freshened on average. The observation of the symmetrical reduction in salinity in NPIW and AAIW/SAMW demonstrates that coherent basin-scale decadal changes do exist in the ocean interior. The question remains as to whether these changes obtained from observing two time periods represent a trend or some natural oscillation in the Pacific climate system. Evidence from sea surface temperature records have shown that the changes that took place in the 1970s and the 1980s in the Pacific (e.g., Trenberth and Hurrell 1994; Graham 1994) are part of a pattern of interdecadal climate variability known as the Pacific Decadal Oscillation (PDO; Mantua et al. 1997). The PDO is centered over the midlatitude North Pacific, and has, during this century alone, changed polarity around 1925, 1947, and 1977. Garreaud and Battisti (1999) have demonstrated that the South Pacific also displays interdecadal (ENSO-like) variability in sea surface temperature, and whose spatial patterns are symmetrical about the equator with their counterparts in the North Pacific. It is entirely possible, that the thermocline and intermediate waters in the North and South Pacific Oceans sampled after 1977 have experienced symmetrically different sea surface conditions due to the PDO and the South Pacific interdecadal variability, when compared to waters before 1977. The average temperature differences in the shallow layers in our observations (see Fig. 6) are comparable to peak SST anomalies of about 0.5°C (e.g., Latif and Barnett 1996), and indeed, the patterns of our observed temperature changes in the upper layers of the North Pacific are akin to the natural oscillation described by Levitus et al. (1994) and Zhang and Levitus (1997).

However, the lack of information on freshwater fluxes associated with the PDO or the South Pacific interdecadal variability means that it is difficult to determine whether our implied surface freshwater redistribution is related to these oscillatory climate phenomena or not. On the other hand, the implied increased freshwater input into the oceans at the subpolar regions, based on our observations, agrees with surface salinity trends from ocean stations in the northeastern Pacific (Freeland and Whitney 1997; Freeland et al. 1997), and is qualitatively consistent with results from coupled climate model experiments with increasing greenhouse gases. Freshening of AAIW during a similar period has also been observed in the Indian Ocean (Bindoff and McDougall 2000), where there are no strong PDO signatures (Mantua et al. 1997). It is therefore tantalizing to speculate that the observed symmetrical freshening of NPIW and AAIW/SAMW represents a trend in the climate system that could be induced by anthropogenic sources. A natural extension to this work would be to investigate whether the freshening of AAIW/SAMW is circumpolar in extent.

Information obtained from this kind of interbasin comparison is useful for validating the effectiveness of coupled atmosphere–ocean models in transmitting atmospheric forcings to the interior of various ocean basins. Although transoceanic sectional comparisons provide information on changes between time snapshots and not as time series, they are useful in providing large-scale information on the spatial nature of water masses changes. This study therefore emphasizes again the importance of top-to-bottom CTD datasets in areas with abundant historical data, and of repeat hydrographic sec-

tions in general, for large-scale climate change detection work in the ocean. The South Pacific Ocean is especially sparse in historical hydrographic data. However, comparison work can be done in the mid- to high latitudes of the South Pacific if the full SCORPIO sections along 28° and 43°S are repeated. These two zonal sections will increase the reliability of the freshwater content change and steric sea level change estimates of the South Pacific. Repeating the 43°S section will also provide more information on recent changes to AAIW and SAMW near their South Pacific formation region.

Acknowledgments. This work was funded by the Australian National Greenhouse Advisory Committee, with extra resources provided by the Antarctic Cooperative Research Centre in Hobart, Australia. Constructive comments from Greg Johnson, Steve Rintoul, and two anonymous reviewers greatly improved the manuscript. We would like to thank Prof. J. Reid for providing the Pacific historical data, and Dr. Harry Bryden for providing the WOCE P21 CTD data. This is a contribution to the World Ocean Circulation Experiment.

REFERENCES

Antonov, J., 1993: Linear trends of temperature at intermediate and deep layers of the North Atlantic and the North Pacific Oceans: 1957–1981. *J. Climate,* **6,** 1928–1942.

Banks, H., J. Bullister, S. Bacon, and H. Bryden, 1995: The deep western boundary current at 17°S in the Pacific Ocean. *Int. WOCE Newsl.,* **19,** 3–5.

Bindoff, N., and J. Church, 1992: Warming of the water column in the southwest Pacific Ocean. *Nature,* **357,** 59–62.

——, and T. McDougall, 1994: Diagnosing climate change and ocean ventilation using hydrographic data. *J. Phys. Oceanogr.,* **24,** 1137–1152.

——, and ——, 2000: Decadal changes along an Indian Ocean section at 32°S and their interpretation. *J. Phys. Oceanogr.,* **30,** 1207–1222.

Bryden, H., M. Griffiths, A. Lavin, R. Millard, G. Parrilla, and W. Smethie, 1996: Decadal changes in water mass characteristics at 24°N in the subtropical North Atlantic Ocean. *J. Climate,* **9,** 3162–3186.

Church, J., J. Godfrey, D. Jackett, and T. McDougall, 1991: A model of sea level rise caused by ocean thermal expansion. *J. Climate,* **4,** 438–456.

Dickson, R., J. Lazier, J. Meincke, P. Rhines, and J. Swift, 1996: Long-term coordinated changes in the convective activity of the North Atlantic. *Progress in Oceanography,* Vol. 38, Pergamon, 241–295.

Douglas, B., 1991: Global sea level rise. *J. Geophys. Res.,* **96,** 6981–6992.

Favorite, F., A. Dodimead, and K. Nasu, 1976: Oceanography of the subarctic Pacific region, 1960–71. *Int. North Pac. Fish. Comm. Bull.,* **33,** 1–187.

Freeland, H., and F. Whitney, 1997: Evidence of secular change in the northeast Pacific Ocean. *Int. WOCE Newsl.,* **26,** 34–36.

——, K. Denman, C. Wong, F. Whitney, and R. Jacques, 1997: Evidence of change in the winter mixed layer in the northeast Pacific Ocean. *Deep-Sea Res. I,* **44,** 2117–2129.

Garreaud, R., and D. Battisti, 1999: Interannual (ENSO) and interdecadal (ENSO-like) variability in the Southern Hemisphere tropospheric circulation. *J. Climate,* **12,** 2113–2123.

Gill, A., 1982: *Atmosphere–Ocean Dynamics.* Academic Press, 662 pp.

Graham, N., 1994: Decadal-scale climate variability in the tropical and North Pacific during the 1970s and 1980s: Observations and model results. *Climate Dyn.,* **10,** 135–162.

Holbrook, N., and N. Bindoff, 1997: Interannual and decadal temperature variability in the southwest Pacific Ocean between 1955 and 1988. *J. Climate,* **10,** 1035–1049.

IPCC, 1995: *Climate Change 1995: The Science of Climate Change.* Cambridge University Press, 572 pp.

Jackett, D., and T. McDougall, 1997: A neutral density variable for the world's oceans. *J. Phys. Oceanogr.,* **27,** 237–263.

Johnson, G. C., and A. H. Orsi, 1997: Southwest Pacific Ocean water-mass changes between 1968/69 and 1990/91. *J. Climate,* **10,** 306–316.

——, D. Rudnick, and B. Taft, 1994: Bottom water variability in the Samoa Passage. *J. Mar. Res.,* **52,** 177–196.

Joyce, T., and P. Robbins, 1996: The long-term hydrographic record at Bermuda. *J. Climate,* **9,** 3121–3131.

——, R. Pickart, and R. Millard, 1999: Long-term hydrographic changes at 52° and 66°W in the North Atlantic subtropical gyre & Caribbean. *Deep-Sea Res.,* **46,** 245–278.

Kessler, W., 1999: Interannual variability of the subsurface high salinity tongue south of the equator at 165°E. *J. Phys. Oceanogr.,* **29,** 2038–2049.

Koltermann, K., A. Sokov, V. Tereschenkov, S. Dobroliubov, K. Lorbacher, and A. Sy, 1999: Decadal changes in the thermohaline circulation of the North Atlantic. *Deep-Sea Res.,* **46,** 109–138.

Latif, M., and T. Barnett, 1996: Decadal climate variability over the North Pacific and North America: Dynamics and predictability. *J. Climate,* **9,** 2407–2423.

Levitus, S., 1982: *Climatological Atlas of the World Ocean.* NOAA Professional Paper 13, 173 pp.

——, J. Antonov, and T. Boyer, 1994: Interannual variability of temperature at a depth of 125 meters in the North Atlantic Ocean. *Science,* **266,** 96–99.

Lozier, M., M. McCartney, and W. Owens, 1994: Anomalous anomalies in averaged hydrographic data. *J. Phys. Oceanogr.,* **24,** 2624–2638.

Manabe, S., K. Bryan, and M. Spelman, 1990: Transient response of a global ocean–atmosphere model to a doubling of atmospheric carbon dioxide. *J. Phys. Oceanogr.,* **20,** 722–749.

Mantua, N., S. Hare, Y. Zhang, J. Wallace, and R. Francis, 1997: A Pacific interdecadal climate oscillation with impacts on salmon production. *Bull. Amer. Meteor. Soc.,* **78,** 1069–1079.

Mantyla, A., and J. Reid, 1983: Abyssal characteristics of the world ocean waters. *Deep-Sea Res.,* **30,** 805–833.

McCartney, M., 1977: Subantarctic Mode Water. *Deep-Sea Res.,* **24,** 103–119.

Olbers, D., V. Gouretski, G. Seib, and J. Schröter, 1992: *Hydrographic Atlas of the Southern Ocean.* Alfred Wegener Institute, 82 pp.

Parker, D., P. Jones, C. Folland, and A. Bevan, 1994: Interdecadal changes of surface temperature since the late nineteenth century. *J. Geophys. Res.* (*Atmos.*), **99,** 14 373–14 399.

Parrilla, G., A. Lavin, H. Bryden, M. Garcia, and R. Millard, 1994: Rising temperatures in the subtropical North Atlantic Ocean over the past 35 years. *Nature,* **369,** 48–51.

Qiu, B., and T. Joyce, 1992: Interannual variability in the mid- and low-latitude western North Pacific. *J. Phys. Oceanogr.,* **22,** 1062–1079.

Read, J., and W. Gould, 1992: Cooling and freshening of the subpolar North Atlantic Ocean since the 1960s. *Nature,* **360,** 55–57.

Reid, J., 1965: *Intermediate Waters of the Pacific Ocean.* The Johns Hopkins Oceanographic Studies, Vol. 2, The Johns Hopkins Press, 85 pp.

Ridgway, K., and J. Godfrey, 1996: Long-term temperature and circulation changes off eastern Australia. *J. Geophys. Res.,* **101,** 3615–3627.

Roemmich, D., 1992: Ocean warming and sea level rise along the southwest U.S. coast. *Science,* **257,** 373–375.

——, and C. Wunsch, 1984: Apparent changes in the climatic state of the deep North Atlantic Ocean. *Nature,* **307,** 447–450.

——, and T. McCallister, 1989: Large scale circulation of the North Pacific Ocean. *Progress in Oceanography*, Vol. 22, Pergamon, 171–204.
——, ——, and J. Swift, 1991: A transpacific hydrographic section along latitude 24°N: The distribution of properties in the subtropical gyre. *Deep-Sea Res.,* **38,** S1–S20.
Schmitz, W., Jr., 1996: On the world ocean circulation. Woods Hole Tech. Rep. WHOI-96-08, 237 pp.
Shuto, K., 1996: Interannual variations of water temperature and salinity along the 137°E meridian. *J. Oceanogr.,* **52,** 575–595.
Sloyan, B., and S. Rintoul, 2001: The Southern Ocean limb of the global deep overturning circulation. *J. Phys. Oceanogr.,* **31,** 143–173.
Suga, T., and K. Hanawa, 1995: The subtropical mode water circulation in the North Pacific. *J. Phys. Oceanogr.,* **25,** 958–970.
——, ——, and Y. Toba, 1989: Subtropical mode water in the 137°E section. *J. Phys. Oceanogr.,* **19,** 1605–1618.
Talley, L., 1991: An Okhotsk Sea water anomaly: Implications for ventilation in the North Pacific. *Deep-Sea Res.,* **38,** S171–S190.
——, 1993: Distribution and formation of North Pacific Intermediate water. *J. Phys. Oceanogr.,* **23,** 517–537.
——, T. Joyce, and R. DeSzoeke, 1991: Transpacific sections at 47°N and 152°W: Distribution of properties. *Deep-Sea Res.,* **38,** S63–S82.
Thomson, R., and S. Tabata, 1987: Steric height trends at Ocean Station PAPA in the northeast Pacific Ocean. *Mar. Geod.,* **11,** 103–113.
Toggweiler, J., K. Dixon, and W. Broecker, 1991: The Peru upwelling and the ventilation of the South Pacific thermocline. *J. Geophys. Res.,* **96,** 20 467–20 497.
Trenberth, K., and J. Hurrell, 1994: Decadal atmosphere–ocean variations in the Pacific. *Climate Dyn.,* **9,** 303–319.
Tsuchiya, M., 1981: The origin of the Pacific Equatorial 13°C Water. *J. Phys. Oceanogr.,* **11,** 794–812.
Warner, M., J. Bullister, D. Wisegarver, R. Gammon, and R. Weiss, 1996: Basin-wide distributions of chlorofluorocarbons CFC-11 and CFC-12 in the North Pacific: 1985–1989. *J. Geophys. Res.,* **101,** 20 525–20 542.
Watanabe, T., and K. Mizuno, 1994: Decadal changes of the thermal structure in the North Pacific. *Int. WOCE Newsl.,* **15,** 10–13.
Whitworth, T., III, B. Warren, W. Nowlin Jr., S. Rutz, R. Pillsbury, and M. Moore, 1999: On the deep western-boundary current in the Southwest Pacific Basin. *Progress in Oceanography,* Vol. 43, Pergamon, 1–54.
Wijffels, S., J. Toole, H. Bryden, R. Fine, W. Jenkins, and J. Bullister, 1996: The water masses and circulation at 10°N in the Pacific. *Deep-Sea Res.,* **43,** 501–544.
Wong, A., N. Bindoff, and J. Church, 1999: Large-scale freshening of intermediate waters in the Pacific and Indian Oceans. *Nature,* **400,** 440–443.
Zhang, R., and S. Levitus, 1997: Structure and cycle of decadal variability of upper-ocean temperature in the North Pacific. *J. Climate,* **10,** 710–727.